International Ocean Discovery Program Expedition 405 Preliminary Report

Tracking Tsunamigenic Slip Across the Japan Trench (JTRACK)

6 September 2024–20 December 2024

Jamie Kirkpatrick, Christine Regalla, Marianne Conin, Patrick Fulton, Kohtaro Ujiie, Shuichi Kodaira, Natsumi Okutsu, Lena Maeda, Sean Toczko, Nobu Eguchi, and the Expedition 405 Scientists

Publisher's notes

Core samples and the wider set of data from the science program covered in this report are under moratorium and accessible only to Science Party members until 20 December 2025.

This publication was prepared by the D/V *Chikyu* Science Operator, the Institute for Marine-Earth Exploration and Engineering (MarE3), at the Japan Agency for Marine-Earth Science and Technology (JAMSTEC) and the *JOIDES Resolution* Science Operator (JRSO) at Texas A&M University (TAMU) as an account of work performed under the International Ocean Discovery Program (IODP). Funding for IODP is provided by the following international partners:

National Science Foundation (NSF), United States
Ministry of Education, Culture, Sports, Science and Technology (MEXT), Japan
European Consortium for Ocean Research Drilling (ECORD)

Portions of this work may have been published in whole or in part in other IODP documents or publications.

Disclaimer

Any opinions, findings, and conclusions or recommendations expressed in this publication are those of the author(s) and do not necessarily reflect the views of the participating agencies, TAMU, or Texas A&M Research Foundation.

Copyright

Citation

ISSN

December 2025

Expedition 405 participants

Expedition 405 scientists

Christine Regalla
Co-Chief Scientist
School of Earth and Sustainability
Northern Arizona University
USA
christine.regalla@nau.edu

Patrick Fulton
Co-Chief Scientist
Deptartment of Earth and Atmospheric Sciences
Cornell University
USA
pfulton@cornell.edu

Jamie Kirkpatrick
Co-Chief Scientist
Geological Sciences and Engineering
University of Nevada, Reno
USA
jkirkpatrick2@unr.edu

Shuichi Kodaira
Co-Chief Scientist
Japan Agency for Marine-Earth Science and Technology
    (JAMSTEC)
Japan
kodaira@jamstec.go.jp

Kohtaro Ujiie
Co-Chief Scientist
Graduate School of Science and Technology
University of Tsukuba
Japan
kujiie@geol.tsukuba.ac.jp

Marianne Conin
Co-Chief Scientist
GeoRessources Laboratory
University of Lorraine
France
marianne.conin@univ-lorraine.fr

Natsumi Okutsu
Expedition Project Manager/Staff Scientist
Institute for Marine-Earth Exploration and Engineering (MarE3)
Japan Agency for Marine-Earth Science and Technology
    (JAMSTEC)
Japan
okutsun@jamstec.go.jp

Lena Maeda
Expedition Project Manager/Staff Scientist
Institute for Marine-Earth Exploration and Engineering (MarE3)
Japan Agency for Marine-Earth Science and Technology
    (JAMSTEC)
Japan
maedal@jamstec.go.jp

Sean Toczko
Expedition Project Manager/Staff Scientist
Institute for Marine-Earth Exploration and Engineering (MarE3)
Japan Agency for Marine-Earth Science and Technology
    (JAMSTEC)
Japan
sean@jamstec.go.jp

Nobu Eguchi
Expedition Project Manager/Staff Scientist
Institute for Marine-Earth Exploration and Engineering (MarE3)
Japan Agency for Marine-Earth Science and Technology
    (JAMSTEC)
Japan
neguchi@jamstec.go.jp

Piero Bellanova
Sedimentologist
Institute of Neotectonics and Natural Hazards
RWTH Aachen University
Germany
p.bellanova@nug.rwth-aachen.de

Cameron Brown
Geochemist
Department of Earth Planetary and Space Sciences
University of California Los Angeles
USA
cbrow133@g.ucla.edu

Morgane Brunet
Sedimentologist
Geo-Ocean
Institut Français de Recherche pour l'Exploitation de la Mer
    (IFREMER)
France

Also at
Institut des Sciences de la mer (ISMER)
Université du Québec à Rimouski
Canada
morganebrunet@hotmail.com

Marissa Castillo
Sedimentologist
Ohio State University
USA
castillo.271@buckeyemail.osu.edu

Yu-Chun Chang
Sedimentologist
Institue of Marine Geodynamics
Japan Agency for Marine-Earth Science and Technology
    (JAMSTEC)
Japan
yuchun@jamstec.go.jp

Mai-Linh Doan
Logging Scientist/Physical Properties Specialist
ISTerre
Université Grenoble Alpes
France
mai-linh.doan@univ-grenoble-alpes.fr

Jenna Everard
Sedimentologist
Department of Earth and Environmental Sciences (Geochemistry)
Lamont-Doherty Earth Observatory
Columbia University
USA
jenna.everard@columbia.edu

Alysa Fintel
Structural Geologist
Earth and Space Sciences Department
University of Washington
USA
afintel@uw.edu

Jonathan Ford
Logging Scientist/Physical Properties Specialist
Department of Geophysics
National Institute of Oceanography and Applied Geophysics—OGS
Italy
jford@ogs.it

Rina Fukuchi
Sedimentologist
Graduate School of Education
Naruto University of Education
Japan
rfukuchi@naruto-u.ac.jp

Amy Gough
Sedimentologist
Institute of GeoEnergy Engineering
Heriot-Watt University
United Kingdom
a.gough@hw.ac.uk

Huiyun Guo
Physical Properties Specialist/Observatory
Division of Geological and Planetary Sciences
California Institute of Technology
USA
hguo2@caltech.edu

Derya Gürer
Structural Geologist
Institute of Earth Sciences
Heidelberg University
Germany
derya.guerer@geow.uni-heidelberg.de

Ron Hackney
Physical Properties Specialist
Research School of Earth Sciences
The Australian National University
Australia
ron.hackney@anu.edu.au

Minori Hagino
Micropaleontologist (radiolarians)
Graduate School of Science and Engineering
Yamagata University
Japan
mhaginores@gmail.com

Yohei Hamada
Structural Geologist/Logging Scientist
Kochi Institute for Core Sample Research
Japan Agency for Marine-Earth Science and Technology (JAMSTEC)
Japan
yhamada@jamstec.go.jp

Hinako Hosono
Structural Geologist
Geological Survey of Japan/AIST
Japan
h.hosono@aist.go.jp

Akira Ijiri
Geochemist
Kobe University
Japan
ijiri@maritime.kobe-u.ac.jp

Matt Ikari
Physical Properties Specialist
MARUM Center for Marine Environmental Sciences
University of Bremen
Germany
mikari@marum.de

Tsuyoshi Ishikawa
Geochemist
Kochi Institute for Core Sample Research
Japan Agency for Marine-Earth Science and Technology (JAMSTEC)
Japan
t-ishik@jamstec.go.jp

Masao Iwai
Micropaleontologist (diatoms)
Marine Core Research Institute (MaCRI)/Kochi Core Center (KCC)
Kochi University
Japan
iwaim@kochi-u.ac.jp

Tamara Jeppson
Physical Properties Specialist
Earthquake Science Center
United State Geological Survey
USA
tjeppson@usgs.gov

Maria-Jose Jurado
Logging Scientist/Physical Properties Specialist
Geosciences Barcelona
Spanish National Research Council (CSIC)
Spain
mjjurado@csic.es

Nana Kamiya
Physical Properties Specialist
 Graduate School of Engineering
 Kyoto University
 Japan
 kamiya.nana.4h@kyoto-u.ac.jp

Toshiya Kanamatsu
Paleomagnetist
 Research Institute for Marine Geodynamics
 Japan Agency for Marine-Earth Science and Technology
  (JAMSTEC)
 Japan
 toshiyak@jamstec.go.jp

Aubrey LaPlante
Structural Geologist
 School of Earth and Sustainability
 Northern Arizona University
 USA
 aal382@nau.edu

Weiren Lin
Physical Properties Specialist
 Graduate School of Engineering
 Kyoto University
 Japan
 hayashi.tameto.6s@kyoto-u.ac.jp

Ayumu Miyakawa
Logging Scientist/Physical Properties Specialist
 Geological Survey of Japan, AIST
 National Institute of Advanced Industrial Science and Technology
 Japan
 miyakawa-a@aist.go.jp

Yuki Morono
Microbiologist/Geochemist
 Kochi Institute for Core Sample Research
 Japan Agency for Marine-Earth Science and Technology
  (JAMSTEC)
 Japan
 morono@jamstec.go.jp

Yasuyuki Nakamura
Core-Log-Seismic Integration
 Research Institute for Marine Geodynamics
 Japan Agency for Marine-Earth Science and Technology
  (JAMSTEC)
 Japan
 yasu@jamstec.go.jp

Uisdean Nicholson
Sedimentologist
 Institute of GeoEnergy Engineering
 Heriot-Watt University
 United Kingdom
 u.nicholson@hw.ac.uk

Hanaya Okuda
Structural Geologist
 Kochi Institute for Core Sample Research
 Japan Agency for Marine-Earth Science and Technology
  (JAMSTEC)
 Japan
 h.okuda@jamstec.go.jp

Pei Pei
Logging Scientist/Physical Properties Specialist
 Laboratoire ISTerre
 Université Grenoble Alpes
 France
 Pei.Pei@univ-grenoble-alpes.fr

Charlotte Pizer
Sedimentologist
 Institute of Geology
 University of Innsbruck
 Austria
 charlotte.pizer@uibk.ac.at

Troy Rasbury
Geochemist
 Geosciences
 Stony Brook University
 USA
 troy.rasbury@stonybrook.edu

Bex (Rebecca) V.M. Robertson
Geochemist
 Department of Earth Science
 Durham University
 United Kingdom
 rebecca.v.robertson@durham.ac.uk

Catherine Ross
Structural Geologist
 Department of Geological Sciences
 University of Colorado Boulder
 USA
 catherine.ross-1@colorado.edu

Sara Satolli
Paleomagnetist
 Department of Engineering and Geology
 University of Chieti-Pescara
 Italy
 sara.satolli@unich.it

Heather Savage
Structural Geologist
 Earth and Planetary Sciences
 University of California, Santa Cruz
 USA
 hsavage@ucsc.edu

Kaitlin Schaible
Logging Scientist/Structural Geologist
 University of Texas Institute for Geophysics
 University of Texas at Austin
 USA
 kaitlin.schaible@utexas.edu

Srisharan Shreedharan
Physical Properties Specialist
 Geosciences
 Utah State University
 USA
 srisharan.shreedharan@usu.edu

Hiroki Sone
Structural Geologist
Civil and Environmental Engineering
University of Wisconsin-Madison
USA
hsone@wisc.edu

Chijun Sun
Geochemist
Department of Earth and Planetary Sciences
University of California Davis
USA
cjsun@ucdavis.edu

Cédric Turel
Sedimentologist
UMR Géoazur
France
turel@geoazur.unice.fr

Taizo Uchida
Paleomagnetist
Graduate School of Integrated Arts and Sciences, Applied Science
    Program
Kochi University
Japan
b24d6a05@s.kochi-u.ac.jp

Asuka Yamaguchi
Sedimentologist
Atmosphere and Ocean Research Institute
The University of Tokyo
Japan
asuka@aori.u-tokyo.ac.jp

Yuzuru Yamamoto
Structural Geologist
Kobe University
Japan
yuzuru-y@harbor.kobe-u.ac.jp

Takeru Yoshimoto
Paleomagnetist
Department of Planetology
Kobe University
Japan
226s422s@stu.kobe-u.ac.jp

Junli Zhang
Geochemist
MARUM Center for Marine Environmental Sciences
University of Bremen
Germany
jzhang@marum.de

Logging Staff Scientists

Adam Wspanialy
Logging Staff Scientist
Institute for Marine-Earth Exploration and Engineering (MarE3)
Japan Agency for Marine-Earth Science and Technology
    (JAMSTEC)
wspanialya@jamstec.go.jp

Erwan Le Ber
Logging Staff Scientist
University of Montpellier
erwan.le-ber@umontpellier.fr

Marisa B. Rydzy
Logging Staff Scientist
University of Leicester
mbr8@leicester.ac.uk

Outreach

Callan Bentley
Outreach Officer
Piedmont Virginia Community College
USA
cbentley@pvcc.edu

Sharon Cooper
Outreach Officer
U.S. Science Support Program
USA
scooper@ldeo.columbia.edu

Will Grant
Outreach Officer
The Australian National University
Australia
will.grant@anu.edu.au

Yoshinori Kurata
Outreach Officer
The National Museum of Emerging Science and Innovation
Japan
yoshinori.kurata@jst.go.jp

Doriane Letexier
Outreach Officer
Freelancer
France
doriane.letexier@gmail.com

Natsumi Miura
Outreach Officer
Office of Science Communication
Miraikan - The National Museum of Emerging Science and
    innovation
Japan
natsumi.miura@jst.go.jp

Maya Pincus
Outreach Officer
U.S. Science Support Program
USA

Nur Schuba
Outreach Officer
University of Texas At Austin
USA
nurschuba@gmail.com

Lisa Smith
Outreach Officer
Curtin University
Australia
lisa.smith1@curtin.edu.au

Videographers

Dan Brinkhuis
Producer
ScienceMedia.nl
Netherlands
dan@sciencemedia.nl

Bram Verlaan
Videographer
Bram Moving Media BV
Netherlands
mail@bramverlaan.nl

Dick Peterse
Outreach Officer
Photography and video–editing
ScienceMedia.nl
Netherlands
peterse@beeldenbeweging.nl

Operational and technical staff

Operation Superintendents (JAMSTEC)

Tomokazu Saruhashi
Ikuo Sawada
Terumichi Ikawa

Drilling Engineers (JAMSTEC)

Noriaki Sakurai
Takahiro Yokoyama
Toru Miyoshi
Yuta Oishi

Operation Geologists (JAMSTEC)

Kan Aoike
Kazuhisa Matsuda

Technical Engineers (JAMSTEC)

Masanori Kyo
Keita Akiyama
Hiroshi Ochi

Captains (Mantle Quest Japan)

Kenichi Inoue
Takumi Maekawa

Offshore Installation Managers (Mantle Quest Japan)

Teruyuki Koyama
Charles Ronald Paul Mcgregor

Laboratory Officers (Marine Works Japan)

Soichi Moriya
Yoshiki Kido
Akihiko Fujihara

Assistant Lab Officers (Marine Works Japan)

Tomonori Watai
Daiki Kawata
Atsushi Kurasawa
Susumu Konno

Curators (Marine Works Japan)

Shigako Nigi
Erii Irie

Laboratory Technicians (Marine Works Japan)

Nobuhiro Anraku
Asami Kikuchi
Marin Sato
Minori Kamikawa
Tomohiro Tani
Ayaka Yonekura
Anvarov Otabek Ulugbek Ogli
Tsumugi Ozawa
Takeru Kochi
Hiroaki Muraki
Toru Fujiki
Ritsuko Sawada
Asaka Kohagura
Paing Zu
Mariko Sano
Hinata Sato
Harumi Toshida
Reiko Nagata
Yasusei Sato
Nahoko Adachi
Yuta Suzuki
Haruna Wakabayashi
Makoto Miyajima
Yasumasa Sakai
Mizuki Imawaka
Kana Miyata
Izumi Miyanishi
Riko Yamauchi
Kazuki Matsuyama
Mana Sakamoto
Shunsuke Nakao
Taichi Nakazato

Publications Specialists (Marine Works Japan)

Akiko Fuse

*At time of publication.

Abstract

The extremely large slip that occurred on the shallow portion of the Japan Trench subduction zone during the 2011 Mw 9.1 Tohoku-oki earthquake directly contributed to the devastating tsunami that inundated the Pacific coast of Japan. International Ocean Drilling Program (IODP) Expedition 405 aimed to investigate the conditions and processes that facilitated the extremely shallow slip on the subduction interface during the 2011 Tohoku-oki earthquake to improve understanding of the factors that slip to the trench on subduction zones. Expedition 405 implemented a combined logging, coring, and observatory operational plan at two sites: Site C0026 ~8 km seaward of the Japan Trench to characterize the input sediments to the subduction zone and Site C0019 ~6 km landward of the trench where the plate boundary fault zone is present at ~825 meters below seafloor (mbsf). At Site C0026, the input section was logged to ~430 mbsf with a logging-while-drilling (LWD) assembly that characterized the succession of sediments and rocks from the seafloor to the basaltic rocks of the oceanic crust. Cores recovered from four holes as deep as 290 mbsf contain a sequence of hemipelagic and pelagic sediments. Site C0019 was previously drilled in 2012 during Integrated Ocean Drilling Program Expedition 343 (Japan Trench Fast Drilling Project [JFAST]), so revisiting this site allowed temporal variations in the frontal prism and plate boundary fault zone to be evaluated. LWD data collected to ~960 mbsf characterized the frontal prism, plate boundary fault zone, and lower plate to the basaltic volcanic rocks. Cores were recovered from multiple holes that contain a variety of muds from the frontal prism and the plate boundary fault zone, as well as lower plate materials. Two borehole observatories were installed at Site C0019 that contain temperature sensors deployed to measure temperature over a period of years and reveal the hydrogeologic structure of the shallow subduction system. These hugely successful drilling operations, combined with postexpedition work to measure the mechanical, frictional, paleomagnetic, and hydrogeologic properties of the core samples and to constrain the history of past seismic slip at Site C0019, provide an unprecedented opportunity to advance our understanding of shallow subduction systems. Thanks to the efforts of a large group of onboard outreach officers and their onshore support, a variety of outreach activities during the expedition leveraged and elevated the success of the operations by sharing the outcomes with diverse domestic and international audiences, including scientists, students, educators, stakeholders, and the general public.

Plain language summary

International Ocean Discovery Program (IODP) Expedition 405 aimed to understand the physical, chemical, and fluid conditions that produced the 2011 Tohoku Japan earthquake and tsunami and to investigate whether any conditions have changed during the past decade that may indicate how the system is preparing for the next event. Two sites were investigated during the expedition: Site C0019, located ~6 km west of the trench, where boreholes were drilled that transected the plate boundary interface and the surrounding rocks and sediment of the upper and lower plates, and Site C0026 on the Pacific plate, ~8 km east of the trench, which was chosen to investigate rock and sediment properties before they enter the plate boundary deformation zone. Geophysical measurements made from within the boreholes and core samples were successfully collected at both sites, and two temperature observatories were installed across the plate boundary at Site C0019 to monitor fluid conditions. These data provide unprecedented opportunity to investigate processes that lead to large magnitude earthquakes and tsunami, not only in the Japan Trench but in similar tectonic settings worldwide. In addition, these expedition objectives and successes were communicated to a broad audience, including scientists, students, teachers, and the general public, through the efforts of several shipboard outreach officers.

1. Introduction

The 2011 Mw 9.1 Tohoku-oki earthquake ruptured a large portion of the Japan Trench subduction zone, resulting in a devastating tsunami that caused thousands of fatalities and billions of dollars in damage in northern Japan (Kazama and Noda, 2012) (Figure **F1A**). The Tohoku-oki earthquake

was the first great subduction event recorded by modern dense geophysical, seismological, and geodetic networks located near the rupture zone. The unprecedented volume of data collected by these networks have allowed scientists to document the spatial and temporal distribution of earthquake slip (Lay, 2018). Together, these data demonstrate that the earthquake was the fourth largest recorded by modern instrumentation and was notable for an exceptional amount of shallow slip in the updip region near to the trench (Kodaira et al., 2020). This large slip at shallow depth contributed directly to the very large (>10 m) tsunami run up experienced along the Sendai and Sanriku coasts. Large near-trench seismic slip has been observed previously (e.g., 1992 Nicaragua and 2006 Java earthquakes) but appears to be relatively rare, emphasizing that our short instrumental and historical records are inadequate to fully characterize the complex and multiscale seismic behavior of subduction zones.

In addition to the integration of seismic and geodetic data, especially from seafloor instruments, drilling through the large-slip region of the earthquake 1 y after the event during Integrated Ocean Drilling Program Expedition 343/343T Japan Trench Fast Drilling Project (JFAST) allowed the first ever glimpse of the fault zone that hosted the slip, as well as an observatory installation that recorded the temperature rise caused by the earthquake. The plate boundary was shown to be localized onto a layer of smectite-rich pelagic clay with multiple slip zones that have hosted earthquake slip in the past (Chester et al., 2013; Ujiie et al., 2013; Kameda et al., 2015; Kirkpatrick et al., 2015; Rabinowitz et al., 2020). The JFAST expedition resulted in three key pieces of information about the 2011 Tohoku earthquake: (1) borehole breakouts showed that shear stress was very low on the plate boundary fault at the time of drilling, suggesting a complete stress drop during the earthquake (Lin et al., 2013); (2) direct measurements of the frictional heat signature across the fault suggest that the fault had very low frictional resistance within the area of large slip (Fulton et al., 2013); and (3) the smectite-rich clay found in the core is sufficiently weak when sheared at
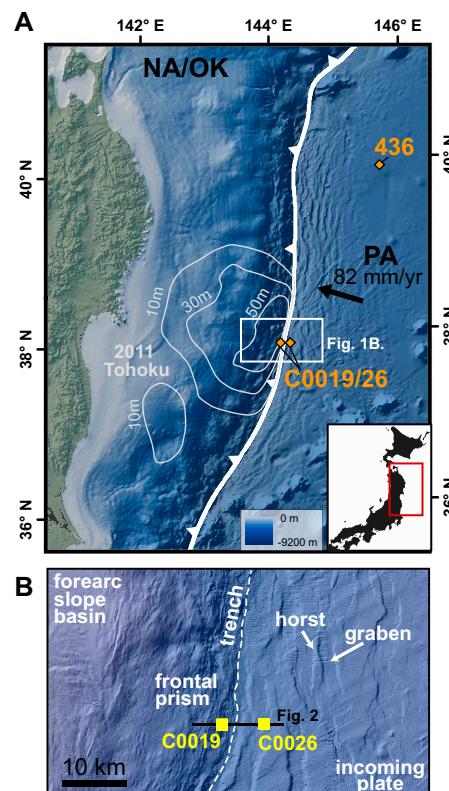

Figure F1. Location maps, Expedition 405. A. Northeastern Japan showing locations of Sites C0019, C0026, and Site 436. White lines = slip contours from 2011 Tohoku-oki earthquake (after Iinuma et al., 2012). EU/OK = Eurasian or Okhotsk plate, PA = Pacific plate. B. Inset map showing major physiographic features of Japan Trench and locations of Sites C0019 and C0026.

seismic slip rate to be consistent with the low stress estimate derived from the temperature data (Ujiie et al., 2013).

Despite the important insights made possible by the JFAST project, there remain critical unanswered questions regarding the physics and recurrence of shallow subduction slip. How fast can a fault heal and reload after a major earthquake? How do we know that the fault captured at JFAST is representative of the shallow structure for the region? How do the properties and distributions of the sediments in the input section on the Pacific plate affect localization of the plate boundary and evolution of the surrounding prism and lower plate? How does the hydrogeologic structure of the plate boundary fault system influence the slip behavior? In addition to providing new insight into the devastating Tohoku-oki earthquake on the Japan Trench subduction zone, addressing these questions can also improve our understanding of other subduction zones around the world, which may have similar earthquake and tsunami hazards.

Expedition 405, which took place from 6 September to 20 December 2024, aimed to investigate the compositional, structural, mechanical, hydrological, and frictional properties of the rocks in and around the shallow plate boundary, and evaluate temporal variations in stress state, fluid flow, and physical properties in the 12 y since the Tohoku-oki earthquake. The expedition focused on two sites, one in the region of large magnitude slip (Site C0019), and the other a reference site on the incoming plate that transected the Pacific plate sediment sequence and oceanic crust (Site C0026) (Figures **F1**, **F2**). Operations took place in three main phases: (1) collection of logging-while-drilling (LWD) data at both sites from seafloor to oceanic crust; (2) coring at Site C0019 across the frontal prism, décollement, and oceanic crust and at Site C0026 across the incoming sediment sequence; and (3) installation of instrument strings to characterize fault zone hydrogeology into two borehole observatories through reinstrumentation of the existing observatory in Hole C0019D (JFAST observatory) and the development and instrumentation of a new observatory in Hole C0019P (Tracking Tsunamigenic Slip Across the Japan Trench [JTRACK] observatory). Together, these logging, coring, and observatory operations provide key data to evaluate the controls on shallow tsunamigenic slip and the temporal variations in stress and physical properties and conditions that occur following a great subduction zone earthquake. This project is directly aligned with the Natural Hazards Impacting Society strategic objective, the Assessing Earthquake
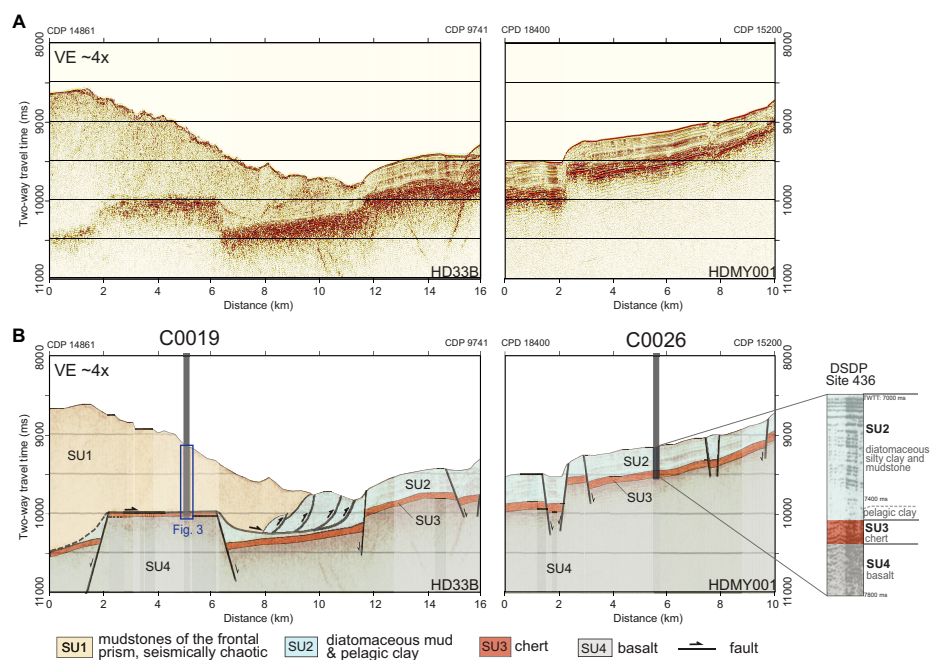

Figure F2. Site survey data, Expedition 405. A. Unannotated high-resolution multichannel seismic reflection Profiles HD33B and HDMY001 showing locations of Sites C0019 and C0026. B. Interpreted seismic line from A showing structure of incoming and overriding plate. Seismic units after Nakamura et al. (2013, 2020) and their correlation to Site 436 (Shipboard Scientific Party, 1980). CDP = common depth point, VE = vertical exaggeration.

and Tsunami Hazards flagship initiative, and the Technology Development and Big Data Analytics enabling elements of the International Ocean Discovery Program (IODP) 2050 Science Framework (Koppers and Coggon, 2020).

2. Background

The Japan Trench subduction zone is defined by an ~8 km deep oceanic trench that marks the location where the Pacific plate subducts beneath northeastern Japan (Figure **F1A**). The plate boundary is defined by a shallowly dipping (~8°) décollement that separates the subducting Pacific plate from the overriding North American/Okhotsk plates (von Huene et al., 1982) at a rate of 82 mm/y (DeMets et al., 2010; Argus et al., 2011). The relatively fast convergence in this region leads to a high rate of seismic activity. Historical records document 13 Mw 7 earthquakes and 5 Mw 8 events over the past 400 y in addition to the 2011 Mw 9 earthquake and its subsequent aftershock sequence (e.g., Hashimoto et al., 2009; Kanamori et al., 2006). Below, we summarize key data supporting the occurrence of shallow slip in the JTRACK transect and results from prior scientific ocean drilling and marine seismic surveys that provide key context for interpreting the results of Expedition 405.

2.1. Shallow slip during the 2011 Tohoku-oki earthquake

The 2011 Tohoku-oki earthquake, observed through one of the world's most advanced seismic, geodetic, and tsunami monitoring networks, has provided crucial insights into fault slip behaviors, including identification of large coseismic slip concentrated in the shallow section of the plate boundary fault (e.g., Lay, 2018). Moreover, differences in the origin of high- and low-frequency seismic energy radiation have been observed (i.e., low-frequency seismic energy radiation concentrated just landward of the trench axis, whereas high-frequency seismic energy radiation originated primarily from the deeper part of the coseismic rupture zone) (e.g., Ishii, 2011; Wang and Mori, 2011).

The aftershock distribution following the earthquake outlined a large coseismic slip zone extending from 35°N to 40°N, spanning the region from the coastline to the trench (Asano et al., 2011). In the area between 37°N and 40°N, aftershocks were located on the seaward side of the trench within the Pacific plate. A striking feature of these aftershocks was the dominance of normal faulting in both the overriding and oceanic plates, contrasting with the reverse faulting activity typical before the earthquake. This shift in seismic behavior is interpreted to reflect the complete stress drop along the plate boundary fault.

Seafloor geodetic measurements, obtained both before and after the 2011 earthquake using the Global Navigation Satellite System–Acoustic (GNSS-A) technique, revealed coseismic deformation of 31 m toward the southeast and a vertical movement of 3 m approximately 50 km landward from the trench (Kido et al., 2011). Furthermore, bathymetric surveys conducted before and after the earthquake, crossing the trench axis, clearly demonstrated that the coseismic seafloor displacement extended to the trench axis. Using the differential bathymetric data, Fujiwara et al. (2011) estimated horizontal displacements ranging 50–56 m and an uplift of 7 m on the trench's landward slope. Complementing these findings, Kodaira et al. (2012) utilized time-lapse seismic survey of before and after the earthquake along the same profile as the bathymetric study to show detailed images of disrupted trench sediments, corroborating the occurrence of trench-breaching coseismic slip. Strasser et al. (2013) analyzed sediment cores, high-resolution bathymetric data, and seismic reflection profiles, concluding that the coseismic fault rupture reaching the trench induced deep-seated rotational slumps.

2.2. Properties of the incoming plate

Prior to Expedition 405, the composition and thickness of units on the incoming Pacific plate outboard of the Tohoku-oki rupture had been determined from coring at Deep Sea Drilling Project (DSDP) Leg 56 and 57 Site 436 located ~250 km north of the JTRACK transect (Figure **F1A**) (Shipboard Scientific Party, 1980) and from mapping of seismic units from multichannel reflection profile data (Nakamura et al., 2013, 2023) (Figure **F2**). Drilling at Site 436 identified three sedimen-

tary units deposited on the oceanic crust of the Pacific plate (Figure F3). The lowest stratigraphic unit was represented in limited core recovery (~40 cm of rubble) by yellow, brown, and reddish brown, veined, brecciated, and occasionally laminated Cretaceous chert (Lithologic Unit 3). These cherts were overlain by 18.8 m of Lower Miocene to Eocene brown to brownish black pelagic clay (Subunit 3A) and 47.5 m of Middle to Upper Miocene yellowish brown radiolarian diatomaceous claystone (Unit 2). The shallowest stratigraphic unit consistent of 66.5 m of partially lithified Late Miocene yellowish green to grayish olive-green vitric diatomaceous silty claystone (Subunit 1B), and 245.5 m of unlithified Holocene to Pleistocene yellowish green to grayish olive-green vitric diatomaceous silty clay and interbedded ash (Subunit 1A).

Shipboard measurements from Site 436 core samples reveal the downhole trends in physical and chemical properties of the incoming plate sediments. Seismic velocities (*P*-wave; discrete samples) increase from 1.5 km/s at the top of the cored interval to 1.65 km/s at the bottom of Lithologic Unit 2 at ~360 meters below seafloor (mbsf). Notably, seismic velocity is much higher (~4.8 km/s) for the small pieces of chert recovered in Unit 3. Porosity is around 70% throughout Units 1 and 2 and decreases to around 55% in the pelagic clay of Subunit 3A. Geochemical profiles from interstitial water (IW) show that, in general, salinity, chlorinity, and calcium concentrations increase with depth, whereas magnesium concentration decreases with depth (Figure F3). However, geochemical data from the pelagic clays of Subunit 3A vary significantly from the overlying units and show a drop in pH and alkalinity and an increase in calcium concentration to approximately double that observed in the rest of the cored interval.

Interpretations of 2D seismic reflection profiles show that the lithologic units identified at Site 436 can be broadly correlated across the incoming plate outboard of the Japan Trench (Nakamura et al., 2013; Fujie et al., 2020; Nakamura et al., 2023). The seismic stratigraphy of the incoming plate stratigraphy consists of three units (Figure F2), the composition of which are interpreted based on comparison with the lithologies recovered in the Site 436 cores: Seismic Unit 4, which correlates to oceanic basalts; Seismic Unit 3, which correlates to chert; and Seismic Unit 2, which correlates to pelagic clay and overlying diatomaceous muds. The thicknesses of Units 2 and 3 are typically <500 m but are variable along the margin. For example, the average sediment thickness is <350 m where the most significant shallow slip occurred during the 2011 Tohoku-oki earthquake (Nakamura et al., 2023).

In addition, seismic reflection data have been used to map the distribution of two units not recovered at Site 436. First, they show trench fill sediments in the axis of the Japan Trench. These sedi-
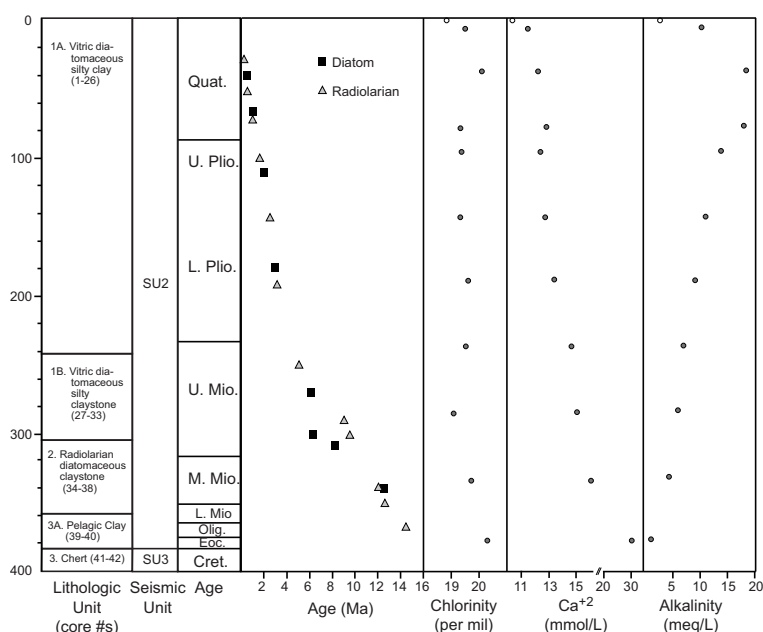

Figure F3. Summary of units, chronology, and selected IW chemistry data, Site 436 (Shipboard Scientific Party, 1980).

ments occur in basins ~50–250 m deep that are laterally segmented by the boundaries of subducted horsts and grabens developed on the incoming plate (Nakamura et al., 2023). Second, these data reveal that petit spot volcanism occurred in isolated volcanic centers on the incoming plate north of the Tohoku rupture area (Hirano et al., 2006, 2019; Fujie et al., 2020; Schottenfels et al., 2023). Petit spot volcanic centers are young (0–8 Ma) mafic volcanic deposits that both break the seafloor and are buried by seafloor sediments, and they are typically <300 m tall by <5 km wide (Hirano et al., 2006; Fujie et al., 2020).

2.3. Properties of the frontal prism and décollement

Prior to Expedition 405, the composition and structure of the frontal prism, plate boundary fault, and lower plate had been investigated using high-resolution multichannel seismic reflection profile data, along with Site C0019 LWD and coring data from Expedition 343 (Expedition 343/343T Scientists, 2013; Nakamura et al., 2013) (Figures F2, F4). These data and the results of postexpedition research following Expedition 343 provide critical context for interpreting Expedition 405 results.

Seismic reflection data show that the frontal prism consists of a low velocity (2–3.5 km/s *P*-wave), seismically chaotic, ~20–30 km wide sedimentary wedge (Seismic Unit 1) (Nakamura et al., 2013, 2020; Kodaira et al., 2017) (Figure F2). Coring through the lower ~200 m of the prism recovered a series of highly disrupted biogenic and siliciclastic mudstones ranging in age from ~0 to 3 Ma,
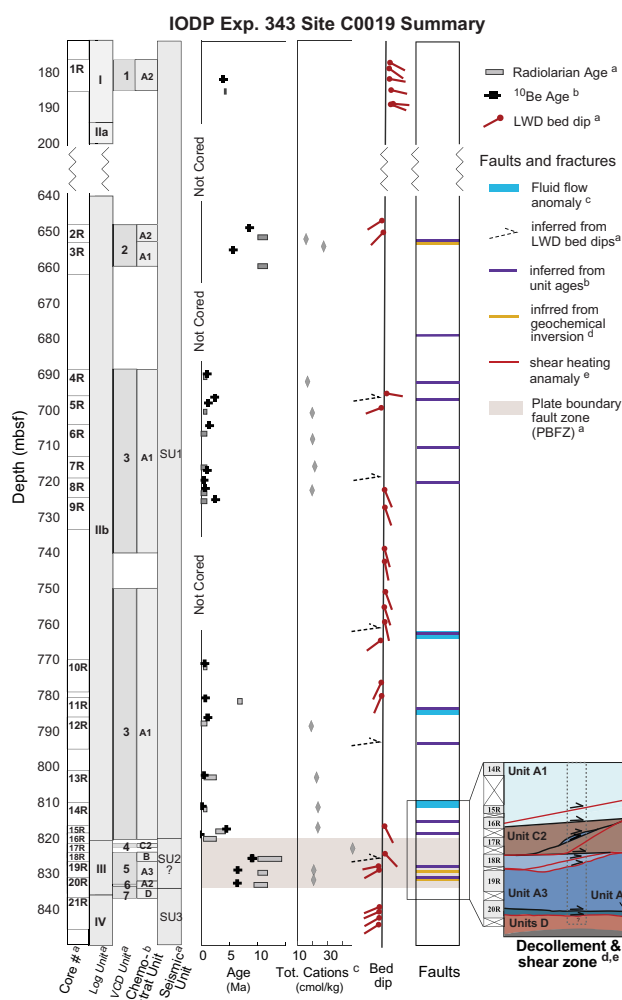

Figure F4. Summary of LWD, core, and observatory data from Expedition 343 Site C0019 that provide information on composition and structures present in the frontal prism. a = Expedition 343/343T Scientists, 2013; b = Regalla et al., 2019; c = Fulton and Brodsky, 2016; d = Rabinowitz et al., 2015; e = Rabinowitz et al., 2020. VCD = visual core description.

with a few intervals as old as ~9 Ma (Expedition 343/343T Scientists, 2013; Rabinowitz et al., 2015; Regalla et al., 2019) (Figure **F4**). LWD borehole resistivity images across the prism showed sequences of tilted beds and fractures with variable resistivity that were interpreted to represent fault-related folds (Expedition 343/343T Scientists, 2013; Chester and Moore 2018) (Figure **F4**). Collectively, these data were interpreted by Expedition 343 scientists to reflect offscraping of a portion of the Miocene to recent biogenic muds on the incoming plate (Seismic Unit 2) to form a structurally complex and seismically chaotic frontal prism (Seismic Unit 1).

Seismic, LWD, and core data from Expedition 343 reveal several major structural and lithologic changes that define the plate boundary fault zone (PBFZ) at Site C0019 (Figure **F4**). Seismic reflection data indicate that the PBFZ separates deformed mudstones of the frontal prism from relatively undeformed, pelagic clays and chert on a horst block on the downgoing plate (Chester et al., 2013; Nakamura et al., 2013). LWD borehole resistivity imagery from Hole C0019B (Figure **F5A**) shows a discrete change in bed dips across the prism from ~60° above the décollement to subhorizontal below the décollement (Expedition 343/343T Scientists, 2013). Gamma ray data from Hole C0019B show an abrupt increase in American Petroleum Institute (API) units, and thus of clay content, from the prism to the PBFZ and an abrupt decrease in API units in the underthrust cherts. Resistivity data across this same zone in Hole C0019B show a decreasing trend within the PBFZ and an abrupt increase in resistivity at the contact with underthrust cherts. Cores recovered from Hole C0019E show the following sequence of units across the lower prism, décollement zone, and lower plate (Expedition 343/343T Scientists, 2013; Chester et al., 2013; Kirkpatrick et al., 2015; Rabinowitz et al., 2015; Regalla et al., 2019). Young (0–2 Ma) biogenic mudstones overlie a ~5 m wide zone of intensely deformed smectite-rich clays containing scaly fabrics and several sharp planar faults. These units in turn overlie a sequence of ~6–12 Ma yellowish brown and grayish brown mudstones that overlie relatively undeformed Eocene to Cretaceous color banded clays and Cretaceous chert. The presence of multiple apparent stratigraphic omissions and inversions implies the PBFZ contains at least eight discrete faults and/or shear zones over a depth range of ~10 m (Expedition 343/343T Scientists, 2013; Chester et al., 2013; Kirkpatrick et al., 2015; Keren and Kirkpatrick, 2016; Regalla et al., 2019; Rabinowitz et al., 2015). The anisotropy of magnetic
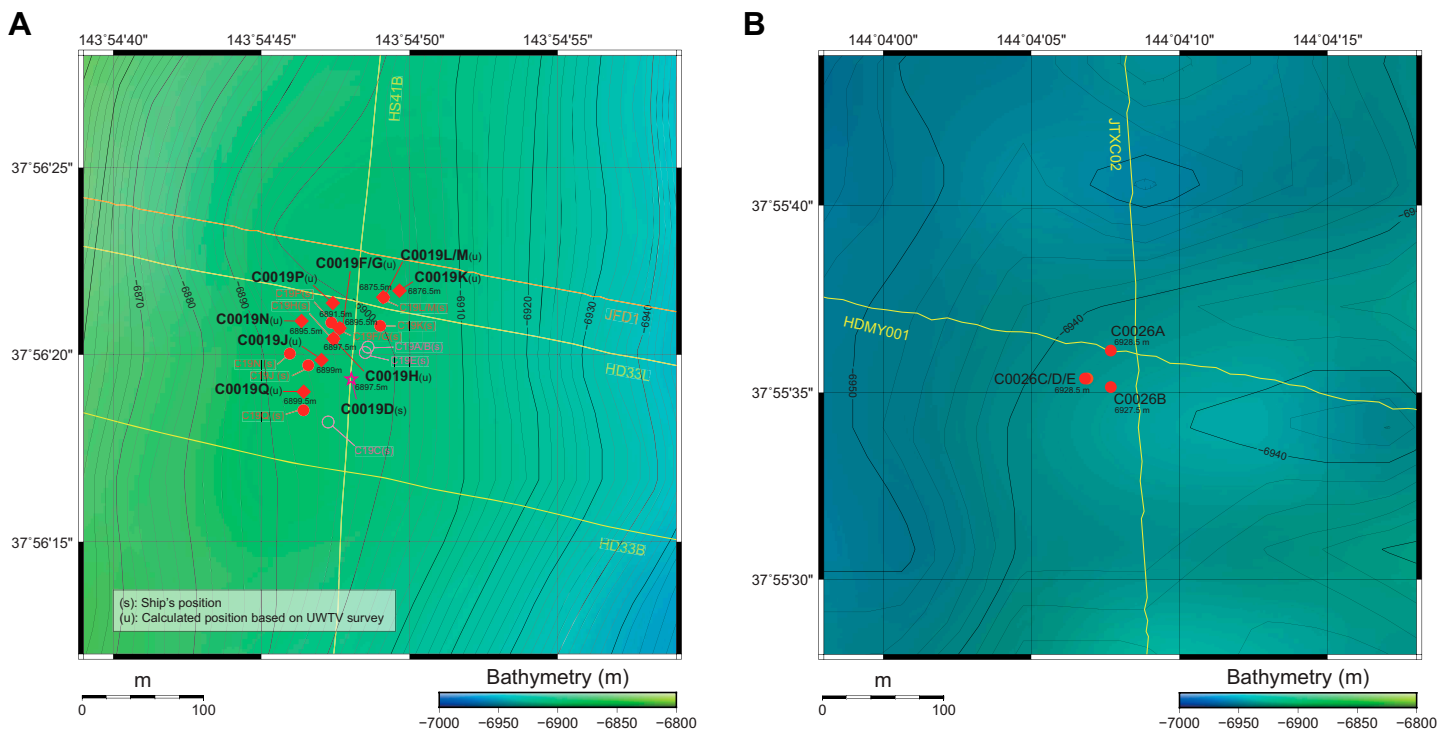

Figure F5. Maps showing locations of holes drilled during Expedition 405. A. Holes C0026A–C0026E and site survey Seismic Lines HDMY001 and JTXC02. B. Expedition 405 Holes C0019E–C0019Q; existing Expedition 343 Holes C0019A–C0019D; and site survey Seismic Lines JDF1, HD33L, HD33B, and HS41. Diamonds = position of ship during drilling, circles = locations of sites on seafloor determined from position of UWTV.

susceptibility in core samples is consistent with horizontal shortening above the décollement but vertical flattening below, suggesting that the décollement is decoupled over geologic time (Yang et al., 2013). Collectively, these data indicate that the décollement zone is ~5–10 m thick and separates deformed Miocene to recent biogenic muds in the prism from relatively undeformed Cretaceous to Eocene pelagic clays and cherts.

2.4. Mechanics and hydrogeology of the plate boundary

Prior to the Mw 9.1 Tohoku-oki earthquake, focal mechanisms in the area indicated that the stress state was predominantly characterized by thrust faulting, with a convergent stress field consistent with the plate motion direction even at shallow depths (Hasegawa et al., 2011). In situ observations of borehole breakouts and measurements of anelastic strain recovery on core samples during the JFAST expedition roughly 1 y after the earthquake revealed that the deviatoric stress in the frontal prism was very low and that the stress state at Site C0019 was in a normal faulting regime with a vertical maximum principal stress axis (e.g., Lin et al., 2013, 2023; Brodsky et al., 2017). These results, in addition to the observed stability of the JFAST boreholes during drilling and observatory installation and the observation of abundant normal faulting aftershocks and of extensional failure at the seabed after the earthquake (e.g., Ide et al., 2011; Tsuji et al., 2011), suggest that the Tohoku-oki earthquake had completely released the plate convergence-parallel shear stress component on the shallow reaches of the plate boundary fault in the region of large coseismic slip (Brodsky et al., 2020).

Friction experiments on cores recovered during the JFAST expedition indicate the smectite-rich pelagic clay within the PBFZ is very weak both statically and dynamically compared to the mudstone above and below the plate boundary fault (Ikari et al., 2015a, 2015b; Remitti et al., 2015; Ujiie et al., 2013). At low slip rates (<1 mm/s), the friction of the plate boundary fault is 0.2–0.26, whereas that of the surrounding mudstone is >0.5 (Ikari et al., 2015b), which likely explains the long-term localization of the plate boundary fault along the smectite-rich pelagic clay. At seismic slip rates, the smectite-rich pelagic clay exhibits an apparent friction coefficient of ~0.1 during ~50 m displacement with a small stress drop, short slip weakening distance, and small fracture energy (Ujiie et al., 2013), which could explain the low resistance to earthquake rupture propagation. The dynamic friction values of the smectite-rich pelagic clay from the plate boundary fault obtained from high-velocity friction experiments are consistent with those obtained from borehole temperature measurements (Fulton et al., 2013) and drilling torque acquired at seismic slip rates (Ujiie et al., 2016).

Observatory, measurement-while-drilling (MWD), and laboratory data from Expedition 343 revealed several key properties of the hydrogeologic structure and evolution of the décollement and surrounding rocks. First, laboratory measurements show that the intrinsic permeability and hydraulic diffusivity are low in prism mudstones and extremely low within the clay-rich plate boundary and underthrust sediments (Tanikawa et al., 2013; Valdez et al., 2014), suggesting fluid flow is controlled by open fractures. Second, thermal recovery data from the 2012 Hole C0019D borehole observatory show evidence for several discrete intervals of high permeability in the 75–100 m above the plate boundary that took significantly longer than surrounding prism to equilibrate from drilling disturbance (Fulton et al., 2013; Purwamaska and Fulton, submitted) (Figure **F4**). Third, high-resolution temperature observatory data acquired over 9 months in Hole C0019D show persistent fluid flow from specific depth intervals within the damage zone above the plate boundary fault (Fulton et al., 2013), suggesting that the prism is overpressured to some degree, driving modest fluid flow into the borehole annulus. Fourth, observatory data show that the hydrogeologic system within the prism appears to evolve over time. Specifically, these data show persistent advective flow at 784 mbsf that subsequently shut off after a large-magnitude local earthquake, accompanied by the emergence of new flow from other channels tens of meters above and below (Fulton et al., 2013). They also show a permeable zone at 792.5 mbsf that appears to have exhibited transient pulses of fluid flow triggered by dynamic shaking associated with numerous regional earthquakes (Fulton and Brodsky, 2016). Fifth, observatory data revealed that no evidence of fluid advection or transient flow was observed within the plate boundary fault at ~819 mbsf in Hole C0019D. Similarly, geochemical data from Hole C0019E show no signs of advection through the fault zone but do reveal depth-dependent trends, suggesting the presence of a sepa-

rate fluid reservoir in the deeper, yet unsampled basaltic crust (Chester et al., 2013; Fulton et al., 2013; Kawagucci et al., 2023). These initial insights into the long- and short-term fluid flow, hydrogeologic structure, and potential damage and healing processes within the PBFZ help motivate JTRACK goals and objectives.

3. Scientific objectives

The overall goal of Expedition 405 is to establish the conditions, rock and fluid properties, and deformation processes within subduction zones that promote large slip to the trench and contribute toward the generation of large tsunamis. To meet this goal, the primary scientific objectives for Expedition 405 are as follows.

3.1. Objective 1: characterize the stress state within and around the fault zone that experienced large coseismic slip during the 2011 Tohoku-oki earthquake

The mechanical conditions in the shallow portion of the subduction zone are critical controls on slip. Objective 1 therefore focuses on constraining the stress field in and around the PBFZ with geophysical measurements and measurements from core samples. This will provide direct insight into the present-day stress resolved on the plate boundary fault and will allow the potential changes in the stress state and accumulation of elastic strain energy since the last in situ measurements in 2012 to be evaluated. Establishing the significance of temporal changes in the stress field will also allow the timescales of damage and healing processes to be assessed. Finally, this objective seeks to confirm that the frictional resistance to slip during the 2011 Tohoku-oki earthquake was a key control on the extreme coseismic slip.

3.2. Objective 2: characterize the geologic composition and structure of the frontal prism, décollement, and subducted oceanic crust to determine how these materials and structures control fault mechanics or reveal evidence of past earthquakes and deformation

Understanding how and why strain becomes localized in the shallow portion of the subduction interface is important for understanding why fault slip during some megathrust earthquakes propagates all the way to the trench rather than terminating at depth or dissipating through distributed deformation. Objective 2 therefore focuses on identification and characterization of the PBFZ and other significant deformation structures, as well as the host rocks in the upper and lower plates. This information will be used to evaluate the influence of fault zone and host rock structures and rock physical properties on deformation and slip. Furthermore, the tendency for slip to the trench will be investigated by identifying past earthquakes in the rock record by applying various proxies for coseismic slip in the sedimentary and deformation structures, which can be used to constrain the paleohistory and recurrence time of large earthquakes and tsunamis.

3.3. Objective 3: characterize the hydrogeology of the plate boundary fault zone and frontal prism

The hydrogeology of the shallow subduction system controls the distribution of pore fluid pressure, which has a direct influence of the effective stresses and the strength of faults and fractures and therefore plays a critical role in earthquake mechanics. Objective 3 focuses on using geophysical borehole data and geochemical measurements from core samples to define the hydrogeologic structure in and around the PBFZ, frontal prism, and lower plate. These measurements will define where fluid flow is presently concentrated and where it has been concentrated in the past, informing variability over time. Installation of a long-term borehole observatory will also show how fault zone hydrogeology responds to external perturbations such as regional earthquakes, providing constraints on the controls on transient fluid flow and monitoring the timescales of hydrologic healing. Overall, this objective will contribute toward developing a better understanding of the relationship between fluids and earthquake physics.

4. Site selection and coring strategy

Expedition 405 visited two sites that were chosen to form a transect across the trench encompassing the reference input section on the Pacific plate and the deformed subduction system beneath the frontal prism in the region of large slip during the 2011 Tohoku-oki earthquake (Figure **F1**). Site C0026 is located ~8 km seaward of the Japan Trench where sedimentary rocks of the Pacific plate overlie basaltic oceanic crust (Figures **F1B**, **F2**). Site C0019 is located ~6 km landward of the trench, above the frontal prism, and was previously visited during Expedition 343 (Figures **F1B**, **F2**).

Site C0026 was selected to allow for characterization of the lithology, chemical composition, mechanical, and hydrologic properties of the sediments and interstitial fluids in the input section. Because these sediments are inputs to the shallow subduction system, the evolution of their properties as they enter the subduction zone is critical to understanding the controls of shallow slip. The location for Site C0026 was chosen based on interpretation of preexpedition seismic reflection profiles (Nakamura et al., 2013). The site is situated between seismically resolvable normal faults that offset sedimentary (Seismic Units 2 and 3) and volcanic rocks (Seismic Unit 4) that accommodate extension associated with flexure at the outer rise (Nakamura et al., 2013; Expedition 343/343T Scientists, 2013) (Figure **F2**). Five holes were drilled at Site C0026 (Figure **F5B**). Operations at Site C0026 included LWD (Hole C0026A) and coring (Holes C0026B–C0026E) across the seafloor sediments to oceanic crust. This site constitutes the second location drilled on the Pacific plate seaward of the Japan Trench, and is the first input site to be drilled directly outboard of the high slip region of the 2011 Tohoku-oki earthquake. Although Site 436 (Shipboard Scientific Party, 1980) described the sediments on the Pacific plate, Site 436 is located >250 km from Site C0026, and seismic reflection surveys document significant lateral variability in the input section (Nakamura et al., 2023). Site C0026 therefore provided a reference section closer to the location of Site C0019 that reduced uncertainty in the stratigraphic correlations and any interpretations regarding changes in physical properties during tectonic burial and additionally provided constraints on the regional-scale variability of the mechanical and hydrologic properties of input material.

Site C0019 lies in the region of large slip of the 2011 Tohoku-oki earthquake. It is located on the lower continental slope near the trench above the frontal prism, which overlies a horst in the subducted Pacific plate (Figures **F1B**, **F2**). Seismic reflection profiles indicate that the frontal prism (Seismic Unit 1) is seismically chaotic with little coherent internal structure. The prism is separated from the lower plate by the PBFZ, which was partially recovered in cores during Expedition 343. The motivation for revisiting this site was to define the deformation structures, lithologies, rock mechanical properties, and interstitial fluid geochemistry of the PBFZ and surrounding rocks in both hanging wall and footwall, all of which are critical controls on long-term strain localization and coseismic slip in the PBFZ. Revisiting this site ~12 y after Expedition 343 also allowed temporal variations in the environmental conditions and rock physical properties to be evaluated. The primary objectives at Site C0019 were therefore to continuously core and log the entire section of Seismic Unit 1 to the depth of refusal in the underlying chert and basalt of the lower plate, including the PBFZ, and to install a long-term borehole observatory to collect a time series of temperature measurements in and around the PBFZ, which will be used to characterize the fault zone hydrogeology and monitor hydrogeologic transients. A total of 10 holes were drilled at Site C0019 (Figure **F5B**). Operations included LWD (Holes C0019F–C0019H), coring of the prism (Holes C0019J–C0019N), coring of underthrust basalt (Hole C0019P), and installation of a borehole observatory (Hole C0019Q).

5. Operations

5.1. Operations strategy

The operations completed during Expedition 405 consisted of the following (Figure **F6**):

- Installing 4½ inch (11.43 cm) tubing with multisensor temperature measurement strings in the existing Hole C0019D and in new Hole C0019Q.
- Drilling a new 8½ inch (21.59 cm) hole using LWD at Sites C0019 and C0026.
- Coring a 10⅝ inch (26.99 cm) hole with the small diameter rotary core barrel (SD-RCB) system and hydraulic piston coring system (HPCS) at Sites C0019 and C0026.

The observatory installation in existing Hole C0019D was part of an Ancillary Project Letter (APL #1013). Rather than installing this observatory at the end of the expedition, the APL was implemented at the beginning as part of an experiment to test for cross-borehole hydrologic communication while drilling. LWD operations in Holes C0019F–C0019H and C0026A followed the observatory installation in Hole C0019D. Because the budgetary impact of the LWD is a significant portion of the entire drilling project, LWD was conducted in series to minimize the onboard tool rental period. The sequence of coring operations was determined based on the prioritization of science objectives; collecting cores from deeper sections, especially the fault zone, was considered to have the highest priority. To follow this prioritization, we first conducted SD-RCB operation in series starting from Site C0019 followed by Site C0026. On the other hand, from the point of view of shallow cores, Site C0026 were prioritized therefore HPCS coring started at Site C0026 and then Site C0019. A new observatory was installed in Hole C0019Q during the last part of the operation because sensor arrangement was finalized based on preliminary results from LWD and coring operations.

5.2. Operations summary

5.2.1. Port call and transit to study area

Expedition 405, JTRACK, began at 1000 h on 6 September 2024, departing from the Port of Shimizu, Shizuoka Prefecture. The drilling vessel (D/V) *Chikyu* arrived at Site C0019 on 7 September and completed all preparations related to setting dynamic positioning by 1530 h 8 September.
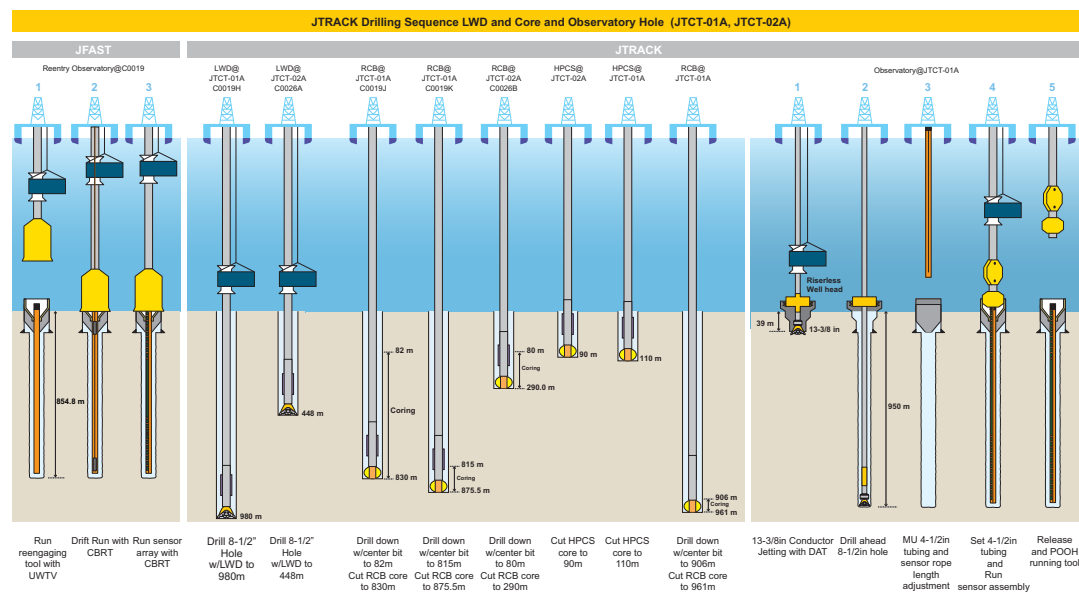

Figure F6. Operations, Expedition 405. CBRT = core barrel retrieving tool. RCB = rotary core barrel, POOH = pull out of hole.

5.2.2. Hole C0019D

Making up and running the Re-engaging Tool to connect to the Hole C0019D wellhead started at 1730 h on 8 September 2024 while drifting from around 4 nmi upstream of the surface current and reached 6353.0 m below rotary table (BRT; 28.5 m above sea level) by 0930 h. The underwater TV (UWTV) camera system was run down at 0930 h on 9 September but was recovered from 2107 m below mean sea level (MSL) due to lost communication with a sonar. The UWTV was run down again at 1845 h after replacing the sonar with a spare one. Running the Re-engaging Tool was resumed when the UWTV reached 6000 m MSL at 2045 h. Seabed survey and searching the wellhead was conducted starting at 0615 h on 10 September. It took almost 13 h to find the wellhead. The Re-engaging Tool was landed on the wellhead at 2030 h. Before running the sensor assembly in the hole, two dummy assembly runs were made to confirm the borehole condition and the bottom depth. Making up and running the sensor assembly in the hole started at 0900 h on 12 September, and then landing the sensor assembly was confirmed at 1715 h. All operations in Hole C0019D were completed when the Re-engaging Tool was pulled to the surface at 1930 h on 13 September.

5.2.3. Hole C0019F

Drilling down without rotating a bottom-hole assembly (BHA) is required to drill a borehole straight down when drilling in ultradeep water, whereas a LWD BHA needs rotation to acquire borehole image data. The target depth for the first LWD hole was 100 mbsf. Making up and running the LWD BHA started at 0000 h on 14 September 2024 and continued to 0100 h on 15 September while LWD signal tests were conducted at 138.0, 3009.0, 6004.5, 6542.5, 6772.5, and 6851.0 m BRT. The UWTV was run down at 0100 h, and a seabed survey was conducted from 0545 to 1000 h. Seabed surveys were initiated by finding Hole C0019D so that it could be used as a reference position. The location for LWD operations was finalized ~30 m north of Hole C0019D. Spud-in of Hole C0019F was achieved at 6924.0 m BRT at 1000 h, followed by washing down to 6934.0 m BRT (10.0 mbsf). Drilling down with rotation started at 1500 h and reached the target depth of 7024 m BRT (100.0 mbsf) at 2145 h (Table **T1**). The LWD BHA was pulled out to 6921.0 m BRT at 2215 h for the next LWD operation.

5.2.4. Hole C0019G

The same ship position for Hole C0019F was used for Hole C0019G because the latter hole targeted a deeper section of the formation. The LWD BHA tagged Hole C0019G at 6924.0 m BRT at 2215 h on 15 September 2024 but showed mud pulse telemetry signal failure from the MWD tool (TeleScope) at 6936.5 m BRT (12.5 mbsf) at 2300 h (Table **T1**). Troubleshooting efforts, including downlink and increasing pump rate to 500 gal/min, were attempted but did not resolve the signal failure. The decision was made to pull the BHA out to the surface at 0130 h on 16 September, and the BHA was recovered on deck at 1900 h.

5.2.5. Hole C0019H

A new LWD BHA was made with the backup TeleScope and mud motor, and it was run in the hole at 1900 h on 16 September 2024. Running down was continued at 0045 h on 18 September while signal tests were conducted at 117.0, 1274.0, 2404.0, 3561.0, 4667.5, 5812.0, and 6837.0 m BRT. The UWTV was run down to 6800 m MSL at 0530 h to finalize hole location. Hole C0019H was established a few meters southwest of Holes C0019F and C0019G at 0657 h on 18 September. Washing down without rotation was maintained to 7016.0 m BRT (90.0 mbsf) at 1215 h. Drilling down with the LWD BHA started at 1700 h after the UWTV was recovered. The LWD BHA reached the target depth of 7906.0 m BRT (980.0 mbsf) at 0730 h on 21 September (Table **T1**) and was pulled out of hole to 7780.0 m BRT (854.0 mbsf). Overpull and hydraulic power swivel (HPS) stall were observed at 7804.0 and 7791.5 m BRT, respectively, while pulling out. Repeat logs were acquired from 7780.0 to 7572.0 m BRT (854.0–646.0 mbsf) and completed by 2130 h. The LWD BHA was recovered on deck at 1700 h on 22 September.

5.2.6. Hole C0026A

The vessel moved from Site C0019 to Hole C0026A by 2115 h on 22 September 2024 and completed preparations for dynamic positioning, such as transponder deployments, calibration, and field arrival check, at 0945 h on 23 September.

The LWD BHA was made up with a new drill bit and the same LWD tools used for Site C0019 operations. It started running at 0945 h. LWD signal tests were performed at 508.0, 2023.0, 5043.0, and 6868.0 m BRT while running. The UWTV camera system was run down to 8 m above the drill bit by 2100 h on 24 September for the seabed survey. The seabed survey was conducted for all planned LWD and coring holes, and it confirmed the water depth for each hole by tagging the seafloor with the drill string. The LWD BHA spudded in Hole C0026A at 6957.0 m BRT at 0019 h on 25 September (Table T1). We washed down from 6957.0 to 7047.0 m BRT (0–90.0 mbsf) without rotation because the first LWD hole of Site C0026 was planned as a deep hole. Drilling started at 1030 h after the UWTV was recovered to the surface and continued to 7405.0 m BRT (448.0 mbsf) at 2200 h on 27 September, with the rate of penetration (ROP) averaging 10–30 m/h.

Table T1. Hole summary, Expedition 405. MSL = below mean sea level, mbsf = meters below seafloor, JST = Japan Standard Time. NA = not applicable.

Hole	Operation	Ship position		UWTV position		Water depth MSL (m)	Number of cores (N)	Coring depth (mbsf)	Interval cored (m)	Core recovered (m)	Recovery (%)	Total depth (mbsf)
		Latitude	Longitude	Latitude	Longitude							
C0019D	Observatory	37°56.3224′N	143°54.8004′E	NA	NA	6897.5	NA	NA	NA	NA	NA	854.8
C0019F	LWD	37°56.3294′N	143°54.7847′E	37°56.3451′N	143°54.7940′E	6895.5	NA	NA	NA	NA	NA	100.0
C0019G	LWD	37°56.3294′N	143°54.7847′E	37°56.3451′N	143°54.7940′E	6895.5	NA	NA	NA	NA	NA	12.5
C0019H	LWD	37°56.3246′N	143°54.7822′E	37°56.3404′N	143°54.7905′E	6897.5	NA	NA	NA	NA	NA	980.0
C0019J	Core (SD-RCB)	37°56.3286′N	143°54.7764′E	37°56.3309′N	143°54.7838′E	6899.0	88	82.0–830.0	748.0	367.5	49.1	830.0
C0019K	Core (SD-RCB)	37°56.3461′N	143°54.8168′E	37°56.3618′N	143°54.8277′E	6875.5	17	815.0–875.5	60.5	41.0	67.8	875.5
C0019L	Core (HPCS)	37°56.3493′N	143°54.8148′E	37°56.3589′N	143°54.8185′E	6876.5	1	0–6.5	6.5	5.3	81.2	6.5
C0019M	Core (HPCS and ESCS)	37°56.3493′N	143°54.8148′E	37°56.3589′N	143°54.8185′E	6876.5	14	0–114.5	114.5	96.0	83.9	114.5
C0019N	Core (SD-RCB)	37°56.3338′N	143°54.7660′E	37°56.3483′N	143°54.7726′E	6895.5	1	901.0–901.3	0.3	0.0	0.0	901.3
C0019P	Core (SD-RCB)	37°56.3476′N	143°54.7894′E	37°56.3563′N	143°54.7902′E	6891.5	5	930.0–946.4	16.4	11.8	71.6	946.4
C0019Q	Observatory	37°56.3086′N	143°54.7747′E	37°56.3168′N	143°54.7738′E	6899.5	NA	NA	NA	NA	NA	925.0
							Total: 126	NA	946.2	521.6	55.1	
C0026A	LWD	37°55.6020′N	144°4.1280′E	NA	NA	6928.5	NA	NA	NA	NA	NA	448.0
C0026B	Core (SD-RCB)	37°55.5857′N	144°4.1280′E	NA	NA	6927.5	32	80.0–290.0	210	102.1	50.9	290.0
C0026C	Core (HPCS)	37°55.5895′N	144°4.1149′E	NA	NA	6928.5	1	0–6.5	6.5	5.9	90.8	6.5
C0026D	Core (HPCS)	37°55.5895′N	144°4.1149′E	NA	NA	6928.5	2	0–6.5	16	6.5	40.5	16.0
C0026E	Core (HPCS)	37°55.5895′N	144°4.1135′E	NA	NA	6928.5	10	0–92.0	92	92.4	100.4	92.0
							Total: 45	NA	324.5	206.9	63.7	

Table T1 (continued).

Hole	Start date (2024)	Start time JST (h)	End date (2024)	End time JST (h)
C0019D	NA	NA	13 Sep	1930
C0019F	15 Sep	1000	15 Sep	2215
C0019G	15 Sep	2215	16 Sep	0130
C0019H	18 Sep	0657	21 Sep	0600
C0019J	5 Oct	0227	24 Oct	0230
C0019K	24 Oct	1630	31 Oct	0930
C0019L	12 Nov	2025	12 Nov	2130
C0019M	12 Nov	2232	15 Nov	2300
C0019N	18 Nov	0815	23 Nov	0545
C0019P	24 Nov	1640	3 Dec	2115
C0019Q	6 Dec	1015	16 Dec	0745
C0026A	25 Sep	0019	1 Oct	1145
C0026B	1 Nov	1558	7 Nov	1400
C0026C	8 Nov	1946	8 Nov	1949
C0026D	8 Nov	2159	9 Nov	0921
C0026E	9 Nov	1035	11 Nov	1545

High torque and stalled pipe were observed, and the drill string stuck at 7401 m BRT just after connecting a new drillpipe stand. Ten cubic meters of seawater gel (SWG) was pumped, followed by multiple attempts to free the drill string until 1000 h on 29 September:

- Overpull of 300 kN observed >30 times while pumping 590 gal/min × 22 MPa;
- Overpull of 300 kN observed >15 times while pumping 590 gal/min × 22 MPa;
- Overpull of 500 kN seen >9 times while pumping 590 gal/min × 22 MPa and 20 kN while pumping 590 gal/min × 22 MPa;
- Sweeping 10 m^3 of SWG with 716 gal/min × 71.9 MPa;
- Jarring down and applying slack off weight 400 kN >15 times, 900 kN overpull and attempt jarring up 15 times without pumping (fire only one time on the fifth attempt);
- 1250 kN overpull and attempt jarring up >100 times while pumping 7 m^3 of kill mud with 600 gal/min × 26.5 MPa;
- Pumping 7 and 10 m^3 of SWG with 600 gal/min × 23 MPa; 1400 kN overpull and attempt jarring up >10 times without pumping.

Because all attempts failed to free the drill string, the final decision to abandon Hole C0026A and LWD operations was made at 1000 h on 29 September. The drill string was severed by a Colliding Tool at 1845 h on 30 September and recovered to the surface at 1145 h on 1 October.

The vessel sailed to an evaluation point soon after recovery of the drill string due to Typhoon 17 (JEBI).

5.2.7. Hole C0019J

The vessel started sailing back to Site C0019 from Typhoon 17 (JEBI) evacuation area at 1100 h on 2 October 2024 while conducting maintenance and preparations for coring operations. A SD-RCB BHA with dual drill collars was made up and run in the hole at 2300 h on 3 October and reached 6832.0 m BRT at 1930 h on 4 October. The center bit was dropped after break circulation, followed by running the UWTV down. A seabed survey was held to confirm the hole location, which was finalized ~30 m southwest of Hole C0019H. Hole C0019J was spud-in at 6927.5 m BRT at 0227 h on 5 October and washed/drilled down with the SD-RCB BHA to the coring starting depth of 7009.5 m BRT (82.0 mbsf). The center bit was recovered at 1930 h, and coring operations began. The first core of this expedition, Core 405-C0019J-1K, was on deck at 0045 h on 6 October. Coring operations continued to 2100 h on 23 October with two interruptions. The first interruption was caused by waiting on weather. The SD-RCB BHA was pulled out from 7209.0 to 6963.5 m BRT (281.5–36.0 mbsf) after recovering Core 21K on deck at 2200 h on 9 October to allow an emergency pull out of the hole in case maintaining dynamic positioning became difficult. The waiting on weather period observed >20 m/s wind (gusts) with ~6 m wave height from 2300 to 0200 h on 11 October. The SD-RCB BHA was then run back to the bottom by 0500 h, and coring operations were resumed. The second interruption occurred after Core 74K was recovered on deck at 0615 h on 20 October. A passing cold front left strong winds and ~6 m wave height on site while the drilling depth approached the estimated depth of the most important formations to be recovered. A short wiper trip was conducted to check and clean the borehole. While pulling the SD-RCB BHA out from 7712.0 to 7450.0 m BRT (784.5–522.5 mbsf), damage was found on the Lower Main Roller on the FWD side of the Traveling Block Dolly at 0900 h. The short trip was resumed after being replaced with a new Main Roller Assembly at 1500 h. Tight spots were observed as discrete peaks in weight-on-bit (WOB) from 7560.0 to 7583.0 m BRT and from 7712.0 to 7715.0 m BRT. To remedy this, the hole was reamed down and then swept out with 10 and 15 m^3 of SWG respectively. Coring resumed at 0030 h on 21 October and reached the target depth at 7757.5 m BRT (830.0 mbsf) at 2100 h on 23 October. Coring advance was set to 9.5 or 10 m for Cores 1K–74K; however, this coring advance was halted to prevent missing or damaging the fragile formation when high standpipe pressure was observed for Cores 75K–88K and instead set to 2.0–4.5 m advance. In total, 88 cores (total length of initial recovery = 367.5 m) were collected from 82.0 to 830.0 mbsf (748.0 m interval) with an average recovery of 49.1% (Table **T1**). The east side of Hole C0019H was cored next to confirm how the formations near the plate boundary were different by location. The SD-RCB BHA was pulled out of Hole C0019J to 6801.0 m BRT by 0200 h on 24 October and kept close to the seafloor while moving to the next hole.

5.2.8. Hole C0019K

The UWTV was run to 6800 m MSL while dropping the center bit at 1530 h on 24 October 2024. Hole C0019K was spud-in ~30 m east of Hole C0019H at 1630 h. The SD-RCB BHA reached 7719.0 m BRT (815.0 mbsf) at 0730 h on 26 October. The center bit was recovered to the surface after a short trip between 7719.0 and 7544.0 m BRT, and coring began from 1445 h and continued until 1115 h on 30 October. Coring advance varied between 2.0 and 6.0 m because of adjustments when standpipe pressure was observed to increase, so that the chances of missing the collection of fragile formations would be minimized. In total, 17 cores (total length of initial recovery = 41.0 m) were collected from 815.0 to 875.5 mbsf (60.5 m interval) with an average recovery of 67.8% (Table **T1**). The SD-RCB BHA was pulled out to the surface at 0930 h on 31 October.

5.2.9. Hole C0026B

The vessel returned to Site C0026 from Site C0019 at 1200 h on 31 October 2024. The SD-RCB BHA was run in the hole and spud into Hole C0026B, which lies ~30 m south of Hole C0026A, at 1158 h on 1 November without the use of the UWTV. The center bit was recovered after washing down from 6956.0 to 7036.0 m BRT (0–80.0 mbsf) at 2215 h. Coring began at 2215 h and continued until 1915 h on 6 November. Coring advance was kept at 9.5 or 10 m for Cores 405-C0026B-1K through 15K and then varied between 3.0 and 7.0 m because of observed standpipe pressure increases to improve the chance of successfully coring fragile formations. In total, 32 cores (total length of initial recovery = 102.2 m) were collected from 80.0 to 290.0 mbsf (210.0 m interval) with an average recovery of 48.6% (Table **T1**). The SD-RCB BHA was pulled out to the surface at 1400 h on 7 November.

5.2.10. Hole C0026C

A HPCS BHA was made up and run in the hole from 2330 h on 7 November 2024 and was spudded into Hole C0026C at 6957.0 m BRT at 1946 h without the UWTV. Core 405-C0026C-1H was recovered on deck at 2100 h (Table **T1**), and it successfully collected the surface sediments and mudline with some bottom water. The HPCS BHA was kept made up in the water as the ship relocated to the next hole.

5.2.11. Hole C0026D

At 2159 h, Hole C0026D was spudded in from the same height and location as Hole C0026C (Table **T1**), again without the UWTV. Core 405-C0026D-1H was recovered on deck at 2315 h and found to have successfully collected the surface sediment and mudline, but the bottom water flowed and was lost when the core barrel was laid down. After cutting the second core, drilling down was required to pull the core barrel out. The sinker bar was recovered but failed to recover the core barrel due to shearing between the sinker bar and the coring line running tool. Attempts were made to recover the core barrel using the backup coring line, and the upper section of the core barrel was recovered. Hole C0026D was abandoned at 0915 h on 9 November because the lower part of the core barrel remained lost in the hole.

5.2.12. Hole C0026E

Spudding in Hole C0026E was conducted at 1035 h on 9 November 2024 at the same height and location as Holes C0026C and C0026D without the UWTV. Core 405-C0026E-1H also collected the surface sediment and mudline with the bottom water. Coring continued with full stroke and required drawworks assist to help pull the inner barrel out for all cores. In total, 10 cores (total length of initial recovery = 92.4 m) were collected from 0 to 92.0 mbsf (92.0 m interval) with an average recovery of 100.4% (Table **T1**). The advanced piston corer temperature (APCT-3) tool was used to measure formation temperature while coring the first 10 HPCS cores from Hole C0026E.

The vessel moved back to Site C0019 after the HPCS BHA was pulled out of the hole at 1545 h on 11 November.

5.2.13. Hole C0019L

The vessel returned to Site C0019 at 1745 h on 11 November 2024. As at Site C0026, at least two holes were planned for HPCS operations to sample the surface sediment and mudline. A HPCS BHA was made up and run in the hole to 6893.0 m BRT at 1100 h on 12 November. A seabed

survey with the UWTV was carried out from 1430 to 1900 h to check the shallow coring hole and prepare for additional planned deep coring operations with the SD-RCB. Hole C0019L was shot from the above the seabed at 2025 h (Table **T1**), and the inner barrel was pulled out by using the drawworks assist. Core 405-C0019L-1H successfully collected the surface sediment and mudline with bottom water by 2130 h.

5.2.14. Hole C0019M

Following Hole C0019L, Hole C0019M was also shot from above the seabed at 2232 h. Core 405-C0019M-1H was retrieved with the mudline and bottom water at 2400 h. Coring continued with full stroke for Cores 1H–6H, although assist from the drawworks was required to pull out the inner barrel. Partial penetration while shooting and overpull while pulling the inner barrel were observed for Cores 7H–10H. Overdrilling while pulling with the drawworks was applied to pull out these cores. Core 10H showed 9.82 m of the initial core length although the coring advance was only 2.5 m. The coring system was changed to the extended shoe coring system (ESCS) for Core 11X. Coring with the ESCS continued through Core 14X with a 9.5 m coring advance. In total, 14 cores (total length of initial recovery = 96.0 m) were collected from 0 to 114.5 mbsf (114.4 m interval) with an average recovery of 83.9% (Table **T1**). The HPCS BHA was pulled out of the hole to the surface at 2300 h on 15 November.

5.2.15. Hole C0019N

To minimize the risk of getting stuck in the hole based on lessons learned from operations in Hole C0026A, a SD-RCB BHA without any drill collars was built up to collect cores below the chert layers. The SD-RCB BHA was made up and run in the hole at 2315 h on 16 November 2024, and it reached 6825.0 m BRT at 2130 h on 17 November. The center bit was dropped before running the UWTV at 0100 h on 18 November. Spud-in of Hole C0019N was performed at 6924.0 m BRT, ~30 m west northwest of Hole C0019H, at 0815 h (Table **T1**), followed by washing down to 6974.0 m BRT (50.0 mbsf). Drilling down with the SD-RCB BHA began at 1530 h after the UWTV was recovered to the surface and continued to 7752.5 m BRT (828.5 mbsf) with an average ROP of ~55 m/h. A short trip was carried out from 7752.5 to 7487.5 m BRT because the ROP decreased from 0430 to 0815 h on 20 November. Drilling paused due to maintenance for a HPS motor malfunction and then resumed again at 1445 h from 7785.5 m BRT. The ROP dropped and became variable with spikes in torque observed. Reaming up and down and sweeping out were performed so that we could continue drilling ahead, but no progress was made from 7825.0 m BRT (901 mbsf). At 0915 h on 21 November, the decision was made to quit drilling ahead instead of coring at the current depth. The center bit was recovered at 1300 h, and we observed that no cutters remained. After circulating and bottoms up, the core barrel was dropped and we attempted to cut a core at 1530 h. The coring barrel was retrieved at 2200 h without any advance. Junk cuttings were found in the core liner, and the decision was made to pull out of the hole. A free-fall funnel was deployed at 0230 h on 22 November, when the BHA pulled out to 7024.0 m BRT (100.0 mbsf). The UWTV was run and recovered to let the free-fall funnel land properly at 1400 h. The BHA was recovered to the surface at 0545 h on 23 November. The top section of the coring bit was found to be severely worn out.

5.2.16. Hole C0019P

We decided the center bit was not strong enough to drill through the chert layers and applied the following operation plan: (1) drill down with a noncoring bit, (2) deploy a free-fall funnel, (3) reenter the hole with the SD-RCB BHA, and (4) core below the chert layers.

The 8½ inch drilling BHA was made and run in the hole at 0745 h on 23 November 2024. The UWTV seabed survey was performed from 1000 to 1630 h on 24 November. The 8½ inch drilling BHA spudded into Hole C0019P at 1630 h and washed down from 6920.0 to 6879.0 m BRT (0–50 mbsf). Drilling down started at 0600 h after the UWTV was recovered to the surface and reached the planned coring depth of 7850.0 m BRT (930.0 mbsf) at 2100 h on 26 November. A free-fall funnel was deployed when the 8½ inch drilling BHA was pulled out to 7020.0 m BRT (100.0 mbsf). Mechanical trouble occurred while pulling out of the hole to 3462.0 m BRT at 1400 h on 27 November. Two bolts connecting the 750T Elevator and Adapter sheared and dropped onto the rig floor. The Elevator was replaced to 500T, and we resumed pulling out the 8½ inch drilling BHA

to the surface at 0500 h on 28 November. The 750T Elevator was repaired with spare parts and set back again at 0345 h on 29 November. The SD-RCB BHA, with a new coring bit and without drilling collars, was made up and run at 0845 h, and it reached 6830.0 m BRT at 0300 h on 30 November. The UWTV found the free-fall funnel at 0730 h and tilted while we attempted reentry at 1200 h. We managed to pass through the free-fall funnel and successfully reentered Hole C0019P at 1730 h while adjusting the vessel position and pushing with the BHA. The UWTV was recovered to the surface at 2100 h, and running the SD-RCB BHA began. The center bit was recovered to the surface at 1015 h on 1 December, followed by conducting circulation and then bottoms up. Coring operations began at 1215 h and the last core was recovered on deck at 2330 h on 2 December. Five cores were collected from 930.0 to 946.4 mbsf (16.4 m interval) with various advances between 0.9 and 5.0 m and an average recovery of 71.6% (Table T1). The SD-RCB BHA was pulled out to the surface at 2115 h on 3 December. With this, all coring operations for this expedition were complete.

5.2.17. Hole C0019Q

The operations to install the temperature sensor assembly consisted of five steps: (1) jetting a 13⅜ inch casing with a 20 inch wellhead; (2) drilling down to the target depth; (3) reentry and running 4½ inch tubing in the hole; (4) running, landing, and releasing the sensor assembly in hole by coring line; and (5) landing and releasing the 4½ inch tubing from the drill string.

Preparing the BHA for 13⅜ inch casing with the 20 inch wellhead, jetting, and drilling ahead tool in one pipe trip (the jetting and DAT BHA) began at 2115 h on 3 December 2024. The vessel moved to Site C0026 and recovered all transponders while preparing the jetting and DAT BHA.

The jetting and DAT BHA was made up and run at 1630 h on 4 December, and it reached 6828.0 m BRT by 0400 h on 6 December. Hole C0019Q was spud into at 6928.0 m BRT at 1015 h after a UWTV seabed survey (Table T1). The 13⅜ inch casing with 20 inch wellhead was successfully jetted into the planned depth of 6970.0 m BRT (42.0 mbsf) at 1415 h. After releasing the DAT was confirmed from the wellhead housing at 2330 h, the UWTV was recovered to the surface at 0400 h on 7 December. The DAT tool drilled from 7567.0 to 7853.0 m BRT (639.0–925.0 mbsf) after washing down to 7003.0 m BRT (75.0 mbsf) at 1230 h on 8 December, followed by short trips between 7853.0 and 7474.0 m BRT and spotting 20 m³ of SWG at 1800 h, and finally was recovered to the surface at 2230 h on 9 December.

A 4½ inch tubing assembly was made up and run starting at 0045 h on 10 December. The UWTV was run to 7 m above the shoe, where the 4½ inch tubing assembly reached 6873.0 m BRT. The Hole C0019Q wellhead was found and reentered the 4½ inch tubing assembly in the hole at 2330 h on 11 December. After confirming the 4½ inch tubing assembly landed on the casing hanger of the wellhead, we attempted to run the sensor assembly. However, the sensor assembly could not pass through the wellhead. The 4½ inch tubing assembly with sensor assembly was pulled out of the hole to the surface, and we found two sensors (#104 and #123) stuck in a narrow part of the casing hanger of the 4½ inch tubing assembly at 1730 h on 13 December.

The 4½ inch tubing assembly was run and reentered Hole C0019Q again at 1800 h on 14 December. The sensor assembly, with a slightly heavier weight of sinker bars (from 15 to 30 kg) to avoid the same kind of failure, was made up and run in hole with pumping, and it successfully landed on the sensor hanger. Jarring down was applied to release the sensor hanger from the sinker bar, and we confirmed the release by coring line tension at 0230 h on 15 December. The hydraulically activated running tool (HART) was activated to release the 4½ inch tubing assembly. Landing and releasing were confirmed visually with the UWTV at 1145 h. Pulling the HART out of the hole to the surface was completed at 0745 h on 16 December.

5.2.18. Transit to Shimizu port

The vessel started to sail back to Shimizu port after all four transponders at Site C0019 were recovered at 1345 h on 17 December 2024 and arrived at the stand-by point off the Port of Shimizu at 1300 h on 19 December. The expedition was completed after docking quayside at the Port of Shimizu at 1000 h on 20 December.

6. Summary of principal results

6.1. Site C0026

Hole C0026A was drilled with a LWD suite of instruments that provided borehole images, resistivity, natural radioactivity (gamma ray) and sonic velocity (for both compressional and shear waves) (Figure F7). Unfortunately, the LWD tools could not be recovered, but MWD data were transmitted in real time with a limited set of LWD, which allowed four logging units to be defined based on their characteristic petrophysical properties: (Unit I) a low resistivity, low gamma ray mudstone layer made up of relatively homogeneous (Unit II) pelagic clays characterized by high gamma ray values, (Unit III) layered chert with low gamma ray and high resistivity and (Unit IV) basalt with very high resistivity and very high sonic velocities (Figure F7). The interpreted lithologies and depth intervals of the logging units correspond closely to the seismic units defined from high-resolution seismic reflection surveys prior to Expedition 405 (Nakamura et al., 2013) and represent the same stratigraphy recovered at Site 436 during Leg 56 (Shipboard Scientific Party, 1980). Few geologic features (bedding and fractures), as well as wellbore failures (breakouts) were identified from real-time resistivity images. However, all features identified in Hole C0026A are of fair quality only, due to the lower data resolution of the real-time images, which limits the possibility of identifying and interpreting individual features.
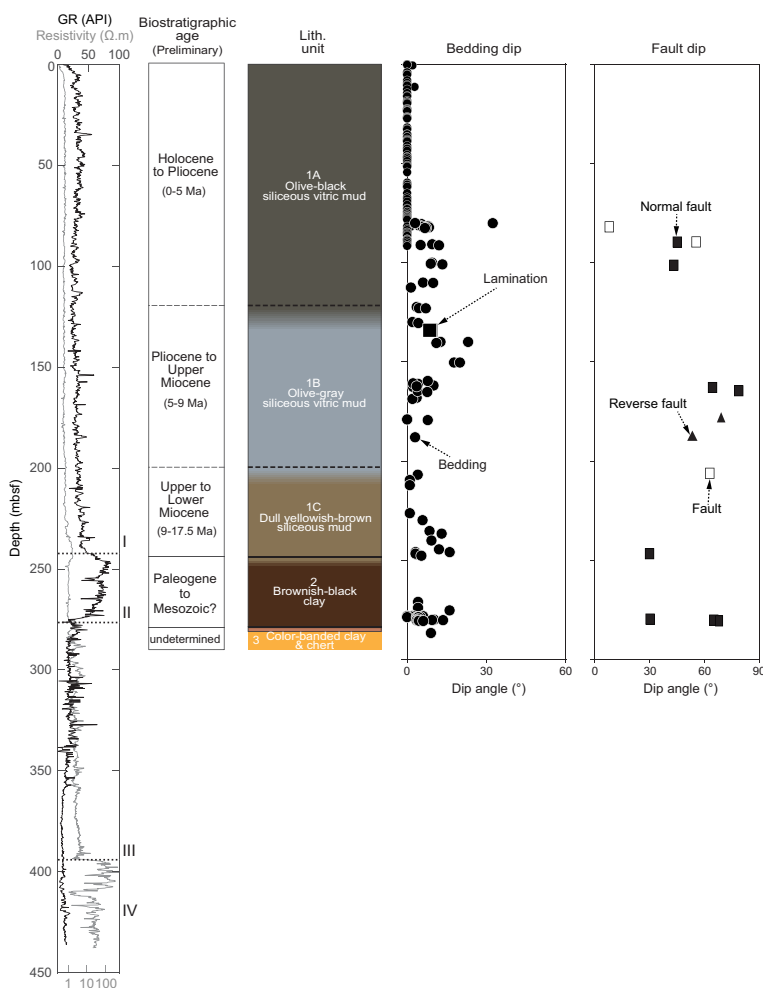

Figure F7. Logging data and visual core description, Expedition 405 Site C0026. Gamma ray (GR) and resistivity (medium) measured with LWD tools (dotted horizontal lines = logging unit boundaries). Lithologic units and summary and structural data are compiled from visual core description of HPCS cores from Holes C0026C–C0026E and SD-RCB cores collected from Hole C0026B. Preliminary biostratigraphic ages from diatom assemblages and initial age-depth profile. Dashed horizontal lines = lithologic subunit boundaries, solid horizontal lines = lithologic unit boundaries.

Three primary lithostratigraphic units were recognized in cores recovered from Site C0026 (Holes C0026B–C0026E) and were distinguished based on visual core descriptions, detailed smear slide analyses, and co-located XRD and XRF analyses (Figure **F7**). Unit 1 is divided into three subunits by color, which, from top to bottom, include Subunit 1A (olive-black siliceous vitric mud), Subunit 1B (olive-gray siliceous vitric mud), and Subunit 1C (dull yellowish brown siliceous mud). These subunits are all muds with compositions that include substantial siliciclastic, volcaniclastic, and biogenic components indicating deposition in a hemipelagic environment. There is a notable decrease in volcanic input from Subunit 1A to Subunit 1C, with a corresponding increase in silici-clastic content. Diatoms and radiolarians are the predominant components of the biogenic material, and the proportion of biogenic components increases with depth until near the base of Subunit 1C, where the biogenic component decreases substantially. The grain size also decreases near the base of Subunit 1C, such that the lithology is silty clay (mud). Unit 2 is brownish black clay characterized by a change to a clay-dominant lithology with notable absence of biogenic components, bioturbation, and volcanic ash layers, although fossilized fish teeth were recovered in Section 405-C0026B-26K-1. Unit 2 is interpreted as pelagic clay that accumulated on the Pacific plate in an area far from continental margins. Unit 3 consists of color-banded clays and lithified chert. The presence of fine-scaled laminae within the color-banded clays suggests minimal transport and/or disturbance of Unit 3. The increasing content of SiO_2 microlite and the transitional occurrence of color-banded clay, porcellanitic clay, and chert from Unit 2 to Unit 3 suggest that silicification/lithification processes are ongoing.

At Site C0026, sediments are generally little deformed and have gentle dips (<30°) at all recovered depths (Figure **F7**). The only deformation structures observed in the shallow cores recovered from Holes C0026C–C0026E are sediment-filled veins, located within ~7–30 cm thick beds at ~13–35 mbsf in Hole C0026E. We interpret the sediment-filled veins as structures related to seismic shaking, consistent with observations and interpretations from other subduction zone margins and analog experiments. Sediment-filled veins were also present in Lithologic Subunit 1C, recovered from Hole C0026B. In Hole C0026B, minor faults with small, millimeter- to centimer-scale offsets predominantly show a normal sense of motion when slip direction can be determined (Figure **F7**). These offset features are primarily seen in Subunit 1A (olive-black silicious vitric mud). Scaly fabric is present between ~245.04 and 246.25 mbsf in the upper portion of the brownish black clay in Unit 2. This scaly fabric is defined by wedge- to discoidal-shaped clay phacoids surrounded by parting surfaces. The dominant deformation structures in Hole C0026B, including the discrete fractures and faults, likely formed as a result of burial and compaction.

Diatoms and radiolarians in samples of cores recovered from Site C0026 were common to abundant, providing tight constraints of the ages of Unit 1 muds as Quaternary to Middle Miocene. Over this time interval, the biostratigraphy of siliceous microfossils revealed the average sedimentation rate was up to 33 m/My in the Pleistocene and Pliocene, whereas average rates were lower in the upper Miocene interval (~5–15 m/My) and very slow during the lower Miocene (<2 m/My). The brownish black clay in Unit 2 below Core 405-C0026B-20K is barren of diatoms. However, sporadic occurrence of radiolarians suggest deposition of the brownish black clay began in the Mesozoic and persisted until the Miocene. The age of the color-banded clay in Unit 3 above the chert was dated by Mesozoic radiolarians genus *Acanthocircus* and *Pseudodictyomitra*. The high abundance of biosiliceous microfossils at this input site may affect the bulk rock porosity.

Both NRM and magnetic susceptibility from Site C0026 show distinct values at the unit level (Figure **F8**). The demagnetization behavior from discrete samples illustrates that the paleomagnetic direction is resolved well, and just a single demagnetization step of archive halves at 20 or 25 mT is a reliable representation of the characteristic component of the magnetization. The natural remanent magnetization (NRM) intensity by 76%–93% after the demagnetization step at 20/25 mT, indicating the presence of a strong drilling overprint that is successfully removed by 10 mT. The anisotropy of magnetic susceptibility (AMS) shows a dominant steep inclination consistent with horizontal layers and a predominance of a sedimentary fabric. In Unit 2, the steeper inclination of the K_{min}, the stronger magnetic foliation, and a higher degree of corrected anisotropy indicate substantial compaction. The good quality of paleomagnetic measurements associated with good recovery provide a high-resolution magnetic polarity record for Hole C0026E sediments (Figure **F8**) and allowed us to constrain an age model based on magnetostratigraphy: the Brunhes/

Matuyama boundary is found at 16.69 mbsf and the Matuyama/Gauss at 87.45 mbsf. Sediments recovered from the lowermost part of Hole C0026B show shallower paleomagnetic inclination, suggesting that Units 2 and 3 (Early Miocene to Cretaceous) were formed at lower paleolatitudes.

The input sediments at Site C0026 are characterized by an almost 200 m thick interval with consistently high porosity, generally between 70% and 80%, that exhibits little to no dependence on depth (Figure F8). Minimal change is observed in the other physical properties measured over this interval, which corresponds to Subunits 1A and 1B and the majority of Subunit 1C. Within Subunit 1C, porosity decreases with depth, accompanied by a slight increase in seismic velocity and electrical resistivity. In Unit 2, the brownish black clay is characterized by an increase in natural gamma radiation (NGR) and a decrease in porosity to ~64%. There is also an increase in anisotropy in electrical resistivity and *P*-wave velocity in Unit 2. In Unit 3, NGR decreases and the Unit 3 color-banded clays and chert exhibit diverse bulk and grain densities. Chert in Unit 3 has the most distinct physical properties, characterized by a significantly lower porosity (one measurement at 12%) and higher seismic velocity and electrical resistivity. In situ temperature measurements and shipboard thermal conductivity measurements between 35.0 and 92.0 mbsf indicate a vertical conductive heat flow of 42.4 mW/m². Overall, the rock physical properties indicate small changes with depth that likely result from compaction, although the largest control is lithology.
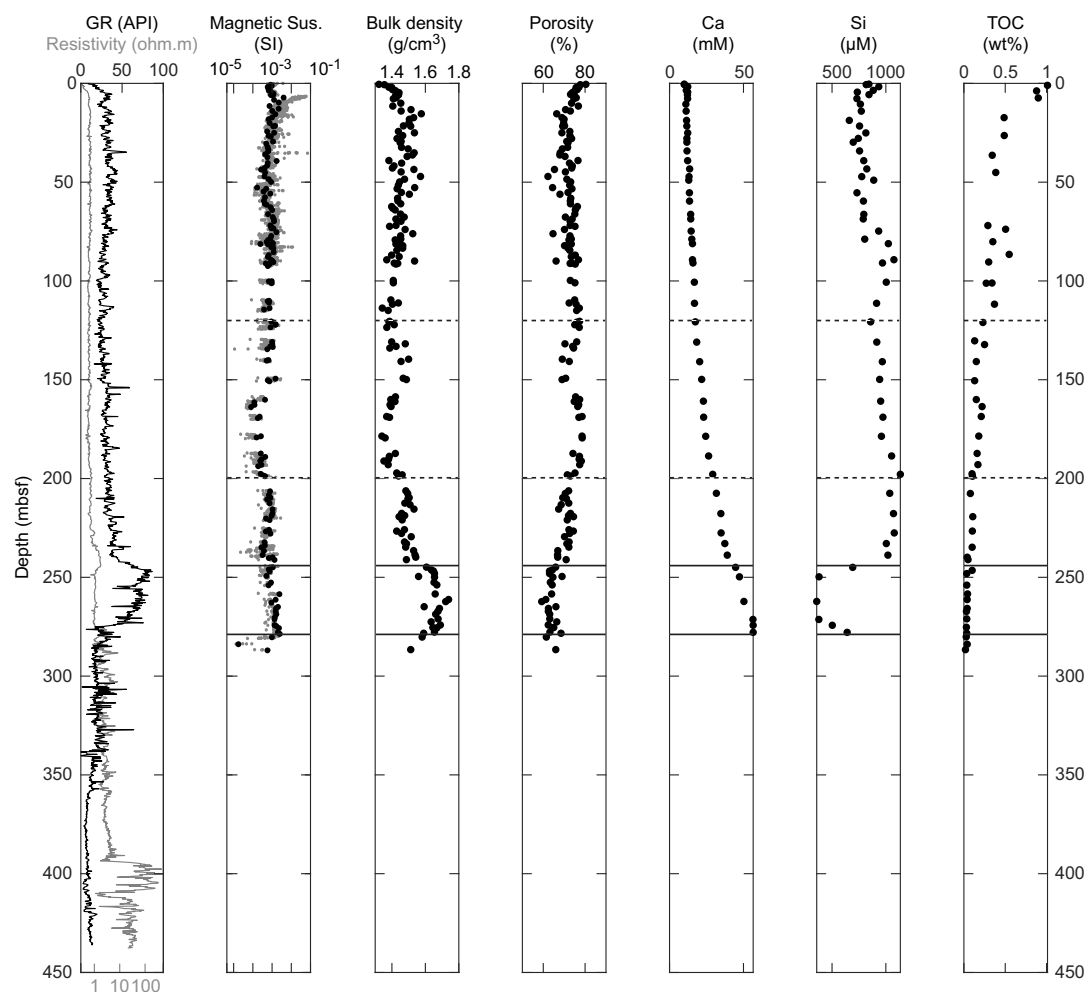

Figure F8. Physical properties and IW geochemistry measurements, Site C0026. Gamma Ray (GR) and resistivity (medium) from Figure F7 are shown for reference. Magnetic susceptibility is shown for continuous measurements on archive half (gray) and discrete sample measurements (black circles). Bulk density and porosity are measured from discrete samples. Preliminary biostratigraphic ages from diatom and radiolarian assemblages and initial age-depth profile. Dashed horizontal lines = lithologic subunit boundaries, solid horizontal lines = lithologic unit boundaries.

The geochemistry of IW and headspace gas from the recovered units at Site C0026 show that concentrations of elements change with depth as well as exhibiting differences from unit to unit (Figure **F8**). In the shallow subsurface, sulfate concentration is consistent with the ambient seawater but decreases rapidly to 23 mM at 14 mbsf. This decrease is likely related to some sulfate reduction, but values stay at this elevated level throughout the cored depths, suggesting that microbial metabolism is only important near the seafloor. Corresponding to the decrease in sulfate, the alkalinity ammonium and phosphate of the IW increases rapidly in the uppermost 14 mbsf and then drops to lower values throughout the rest of the cored interval, whereas chlorinity is near seawater values near the seafloor and increases slightly to about over the next 20 mbsf where it remains relatively stable within Unit 1.

IW sodium (Na), potassium (K), and magnesium (Mg) concentrations near the seafloor in Hole C0026D show relatively scattered values both higher and lower than ambient seawater. These IW Na, K, and Mg values converge to seawater-like values at 10–30 mbsf and then gradually decrease with depth. On the other hand, IW calcium (Ca) and strontium (Sr) concentrations show seawater-like values near the seafloor and increase monotonically with depth (Figure **F8**). IW lithium (Li) and boron (B) concentrations show variability throughout Site C0026, likely reflecting diagenetic uptake or release. Silica (Si) concentrations increase with depth with some fluctuations from 730–930 μM at <15 mbsf to 1,000–1,130 μM at 200–240 mbsf. The abundance of diatom frustules and sponge spicules in the smear slide descriptions can account for the very high dissolved Si concentrations. Below 240 mbsf in Unit 2, the IW Si concentrations decrease abruptly to 360–690 μM and then increase abruptly again below Unit 2. Unit 2 is notable for a lack of silica bearing microfossils, but a corresponding decrease in K may signal clay mineral or zeolite formation. Redox-sensitive elements manganese (Mn) and iron (Fe) show large variations at Site C0026 that are surprising relative to the elevated sulfate values which suggest oxidizing conditions. The Mn value increases rapidly with some fluctuations to a peak in Lithologic Subunit 1C but decreases dramatically into Unit 2. The IW in Unit 2 is also depleted in Fe, further suggesting a control by Fe-Mn oxide phases. IW barium (Ba) concentrations are less than 1 μM throughout the Site C0026 cores, consistent with elevated sulfate throughout the cores, which would limit Ba solubility due to barite formation. Headspace gas methane concentrations are less than 10 ppm and decrease with depth to 2 ppm near the bottom of Hole C0026B. Ethane, propane and *n*-butane are all below detection limits at all depths. Consistent with the low headspace gas concentrations, total organic carbon (TOC) contents are generally low and exhibit a general decrease with depth (Figure **F8**). Calcium carbonate is low throughout the cores at Site C0026.

Sampling and subsampling for microbiology was completed in Holes C0026B–C0026E. A total of 19 whole-round samples were collected from the cores, and residue from 50 IW squeeze cakes were collected for cross-comparison. In addition, 7 drill fluid samples and 20 core liner fluid samples were also collected to analyze samples for possible microbial contamination. A minimized subsampling routine was applied to cores from Site C0026 due to the lack of a microbiologist onboard during this coring phase. The remainder of the microbial analyses took place postexpedition.

6.2. Site C0019

Logging data were acquired using an LWD/MWD assembly in Holes C0019F (to 86 mbsf) and C0019H (to 980 mbsf) that provided ultrahigh-resolution borehole images, resistivity, natural radioactivity (gamma ray) and sonic velocity measurements (for both compressional and shear waves) (Figure **F9**). Five logging units were defined from a combination of different LWD measurements, particularly gamma ray, resistivity and sonic logs. Logging Unit I is interpreted as mudstone characterized by moderate gamma ray values, very low resistivity and low *P*-wave velocity (V_P) values, with both V_P and resistivity values increasing slightly with depth, consistent with a burial compaction trend for unconsolidated sediments. Unit II is interpreted as mudstone characterized by slightly higher gamma ray, resistivity, and V_P values compared to Unit I, although the lower portion of Unit II has generally lower gamma ray values and resistivity values compared to the upper portion. Units I and II at Site C0019 constitute a package of low-resistivity and low sonic velocity material similar to Unit I at Site C0026, but with a larger thickness. Unit III is characterized by an interval of high gamma ray values and a gradual downhole decrease in resistivity and V_P,

and it occurs at a depth consistent with the PBFZ. Unit IV is characterized by a sharp decrease in gamma ray values and a significant increase in resistivity. Borehole images show alternating layers of lower and higher resistivity, suggesting this unit consists primarily of chert. Unit V is characterized by an abrupt increase in gamma ray values, resistivity, and V_P compared to Unit IV, and borehole images show features interpreted as pillow lavas, and cooling fractures, typical of basaltic rocks. Unit V also contains two intervals with low gamma ray and lower resistivity, which are similar to Unit IV. Therefore, Unit V is interpreted to be a sequence of volcanic rocks intercalated with sedimentary rocks, potentially chert. Based on the similarities in petrophysical characteristics of the units, as well as the relative positions, Units IV and V at Site C0019 are correlated with Units III and IV from Site C0026, respectively. In the upper plate (Units I and II), borehole images show several fractured intervals, and bedding with moderate to very steep dips, which contrasts with the shallow dipping beds in the PBFZ (Unit III) and the sediments of the downgoing plate (Unit IV). The PBFZ is identified from the lithological signature, notably the high gamma ray interval, and the change of bedding dips, but no clear individual structure could be identified as the décollement fault on the borehole images. Breakouts are mainly localized in a narrow interval in Unit II, more than 100 m above the PBFZ.

The lithostratigraphy of Site C0019 can be summarized as three sections based on their composition and the structural context from which they were recovered: (1) olive-black and gray siliceous vitric mud(-stone) above the PBFZ (Units 1–6 in Holes C0019J and C0019L–C0019N and Unit K1
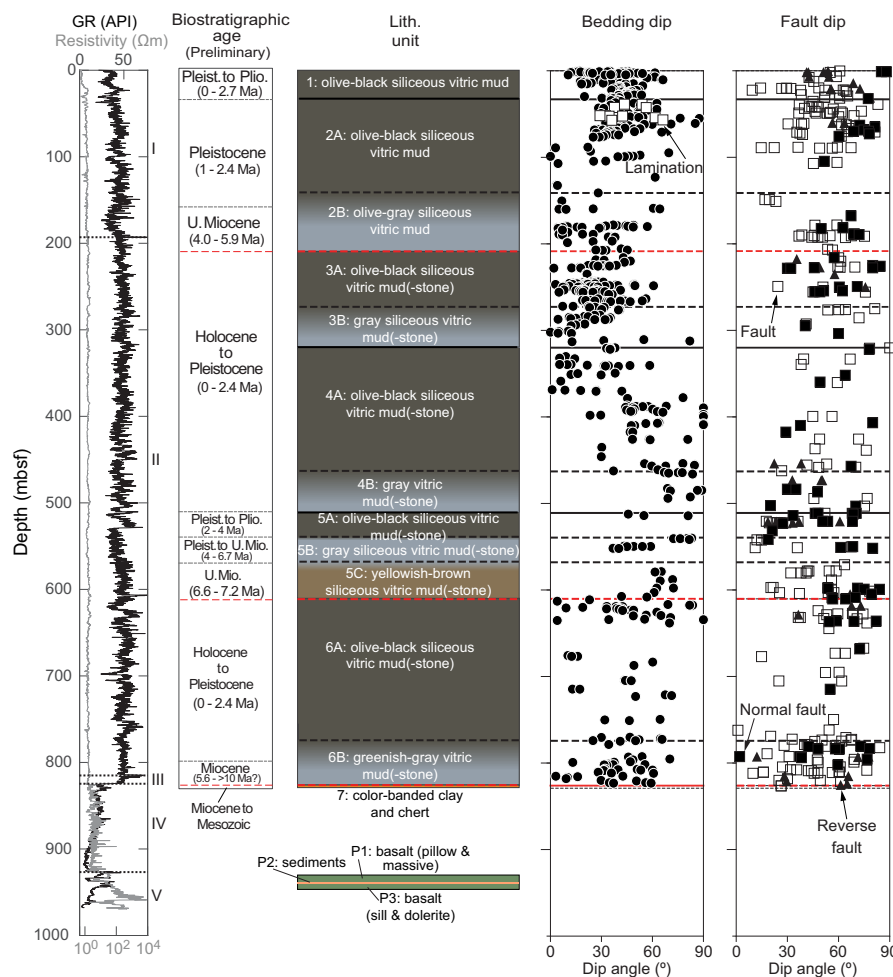

Figure F9. Logging data and visual core description, Expedition 405 Site C0019. Gamma Ray (GR) and resistivity (medium) measured with LWD tools (dotted horizontal lines = logging unit boundaries). Lithologic units and summary and structural data are compiled from visual core description of HPCS cores from Holes C0019L and C0019M and SD-RCB cores collected from Holes C0019J and C0019K. Dashed horizontal lines = lithologic subunit boundaries, solid horizontal lines = lithologic unit boundaries, red lines = major faults as detailed in Site C0019.

in Hole C0019K), (2) brownish black clay (Unit K2) transitioning to chert (Unit 7 and Unit K3) beneath the PBFZ, and (3) basalt and sedimentary rocks of the basement of the underthrust Pacific plate (Unit P1-3) (Figure **F9**). The sediments recovered from above the plate boundary (Lithologic Units 1–6 and K1) resemble at least five repeating sequences of Pleistocene to Miocene olive-black to gray (and for Unit 5 to dull yellowish brown) siliceous vitric mud. Each sequence is divided by either a distinctive unit boundary or fault plane. Additionally, some unit boundaries represent significant age inversions (e.g., Subunit 2B/3A and 5C/6A boundaries). The sediments are generally compositionally similar to the lithologies found at Site C0026. However, there are distinct differences from Site C0026, such as the common presence of mass transport deposits (MTDs) in the Site C0019 sediments, illustrated by chaotic and inclined bedding and other soft-sediment deformation features, potentially resulting from deformational processes and slope instability, as well as the presence of calcareous nannofossils and calcite in specific intervals of the chaotic lithologies. In contrast to the prism, the footwall beneath the PBFZ consists of sediments of early Late Miocene and older, although the recovered sediments below the plate boundary show heterogeneity, highlighted by the different stratigraphic sequence between Holes C0019J and C0019K. In Hole C0019J, color-banded clays and chert are present directly below the plate boundary and the brownish black clay (Unit K2) is not preserved. However, Hole C0019K corresponds to the similar lithologic sequence encountered at Site C0026, with brownish black pelagic clays (Unit K2) underlain by color-banded clays and chert (Unit K3). The deepest cores recovered (Hole C0019P) below the chert exhibit the basalt basement with interlayered sedimentary rocks (e.g., limestone, mudstone, and chert) of the subducted Pacific plate. This sequence illustrates the oceanic crust of the subducting Pacific plate.

Cores recovered from Site C0019 contain sediments with a very wide range of gently to steeply dipping beds (0–90°) (Figure **F9**). Deformation structures are present throughout the cored interval, including major reverse faults, minor faults with reverse and normal slip, fractures, fracture networks, sediment-filled veins, dark seams and dark seam networks, and scaly fabric. Notably, three major faults were encountered at Site C0019: a fault inferred at ~207 mbsf, a fault at 610 mbsf, and the plate boundary fault at 826 mbsf (Hole C0019J) and 846 mbsf (Hole C0019K). The ~207 mbsf fault is inferred from an age reversal seen in the biostratigraphy, as well as a change in physical properties, but no obvious fault zone structure occurs within the cores, likely due to incomplete core recovery. The 610 mbsf fault is characterized by an orange breccia and scaly fabrics in the hanging wall, a transitional boundary with a gray gouge layer, and a gray mudstone in the footwall. Juxtaposed against the transitional gray gouge layer is a thin, centimeter-scale, black layer that is inferred to be a localized slip zone. In general, there is an increase in the density of deformation structures near the boundaries of major faults. Between these faults, bedding dips increase downcore, from gently to steeply dipping, which correlate well to bedding dips measured from LWD. This general downcore steepening of bedding dips is inferred to be due to a large-scale fold (tens to hundreds of meters) within the accretionary prism.

At the base of the frontal prism, the PBFZ is marked by a sharp contact at the base of the Miocene Lithologic Subunit 6B greenish gray siliceous vitric mud(-stone) at 826 mbsf (Hole J) and Lithologic Unit K1 olive-gray vitric mud(-stone) at 846 mbsf (Hole C0019K) (Figure **F9**). The PBFZ comprises mudstones and clays and contains several millimeter- to centimeter-scale discrete slip zones, as well as intervals of penetrative scaly fabric, fault breccia, and gouge. There are minor variations in the deformation structures of the plate boundary fault between Holes C0019J and C0019K. Overall, the fault in Hole C0019J is ~87.5 cm thick and ends at an interval of intercalated yellowish brown clay and chert. Similarly, in Hole C0019K, the discrete fault zone consists of ~83 cm of sheared clays and mudstones and shares a basal contact with ~25 m of brownish black clay that contains a scaly fabric. This interval of brownish black scaly clay is underlain by intercalated yellowish brown clay and chert, correlated to the unit at the base of Hole C0019J.

In Hole C0019P, the recovered basalt has abundant, millimeter- to centimeter-thick calcite veins. Cross-cutting relationships and crack-seal textures imply multiple episodes of veining. An injection feature was documented in Core 405-C0019P-1K (930.7–932.0 mbsf) that included pink carbonate, white carbonate, and green-filled veins. The basalt was otherwise undeformed, and there was no evidence of shear deformation.

Biostratigraphy of siliceous microfossils (especially diatoms) clearly documented the frontal prism structure and constrained the locations of major faults. Overall, the ages of the sediments in the prism range from Pleistocene to Miocene, although in general there are few intervals that show coherent age-depth trends. Major reversals defined faults at ~210, ~610, and the PBFZ at ~826 mbsf. Most prism units contain diatoms with Pleistocene, Pliocene, and upper Miocene ages that are interpreted as evidence for deposition by slope deformation processes, soft-sediment deformation, and MTDs. Biostratigraphic constraints suggest MTD thickness is up to ~300 m. In addition, the sporadic occurrence of radiolarians suggests a part of the brownish black clay (Lithologic Unit K2) was deposited during the Miocene, and the chert above the basalt is Mesozoic.

Paleomagnetic investigations combined archive-half measurements with measurements of discrete samples (Figure **F10**). Following removal of a steep low-coercivity component due to drilling overprint, the characteristic remanent magnetization (ChRM) is successfully isolated between 15 and 20 mT and 80 mT in sediments. Some samples show an intermediate coercivity component and/or a gyroremanence, which possibly indicates the presence of pyrrhotite or greigite. The basalt samples show two components: a softer one demagnetized up to 20 mT and a harder one completely demagnetized between 50 and 80 mT. The demagnetization step at 20/25 mT of archive sections is a reli-
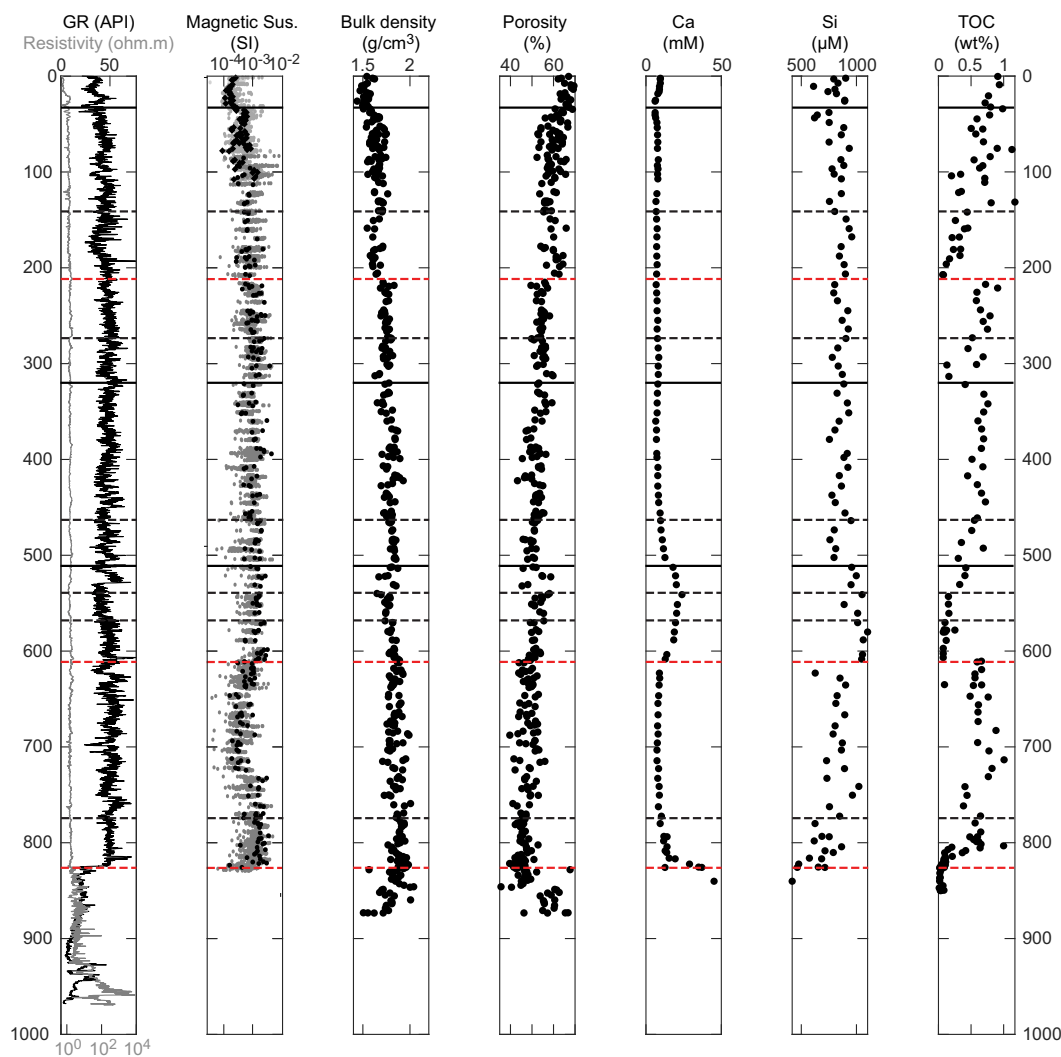

Figure F10. Physical properties and IW geochemistry measurements, Site C0019. Gamma Ray (GR) and resistivity (medium) from Figure F9 are shown for reference. Magnetic susceptibility is shown for continuous measurements on archive half (gray) and discrete sample measurements (black circles). Bulk density and porosity are measured from discrete samples. Dashed horizontal lines = lithologic subunit boundaries, solid horizontal lines = lithologic unit boundaries, red lines = major faults as detailed in Site C0019.

able representative of the primary component, save for the sedimentary rocks from Hole C0019P that show a very strong coercivity due to the presence of (titano-)hematite. The AMS shows the predominance of a flattening fabric, but there are also distinct variations of the AMS parameters with depth, and samples with high scatter may be due to MTD deposits. A decrease of the corrected degree of anisotropy (Pj) is observed above all the major fault zones. Unit K2 shows very similar magnetic fabric to the lithologically similar Unit 2 at Site C0026. Because the magnetic directions vary depending on the dip direction and dip angle of the bedding and the inclinations are biased toward positive values, it was not possible to reconstruct a reliable magnetostratigraphy for Site C0019. Although we don't lack exact age constraints, the Mesozoic horizontal layers from Lithologic Units K2 and K3 are characterized by inclinations shallower than the expected values at the site coordinates, suggesting sedimentation at low paleolatitudes. In the basalts, inclinations between 0° and 10° indicate that they formed close to the equator. The Königsberger ratio is greater than 1, indicating that the total magnetization of the recovered basalts is contributing to the oceanic magnetic anomalies in this area.

At Site C0019, the frontal prism is characterized by an overall decrease in porosity and concomitant increase in bulk density with depth (Figure **F10**). NGR and thermal conductivity are relatively constant, and discrete electrical resistivity and wave velocity values display a slight increase with depth. The interval between the interpreted fault at ~610 mbsf and the PBFZ is marked by increased scatter in the measurements of porosity and bulk density, as well as higher anisotropies in discrete electrical resistivity and wave velocity. Below the PBFZ, the brownish black clay (Unit K2) has an increased NGR (~60–90 counts/s) and near constant porosity (~58%) and anisotropic electrical resistivity and velocity. In the color-banded clays (Unit 7 and K3), NGR decreases and porosity initially remains high but the porosity decreases and wave velocity increases as the clays become semilithified. The lowest porosities and highest discrete velocities and electrical resistivities at Site C0019 were measured in the chert. The porosity in the chert is ~3%, whereas the igneous rocks from Hole C0019P have an average porosity of 14.5% and reach up to 21.4%. In situ temperature measurements and shipboard thermal conductivity measurements between 23.5 and 67.5 mbsf indicate a vertical conductive heat flow of 32.0 mW/m^2.

At Site C0019, the IW geochemistry and headspace gas profiles show rapid changes in salinity, pH, sulfate, alkalinity, ammonium, phosphate, bromide, and methane in the uppermost 100 m of the sediments, with characteristics indicative of high microbial organic matter degradation. Below this microbially intensive upper layer, TOC exhibits consistent patterns of changes around the three identified faults around 207, 610, and 826 mbsf (Figure **F10**), showing gradual decreases toward nearly 0 wt% immediately above the faults, below which TOC concentrations dramatically shift to high values. However, other geochemical data exhibit different behaviors at the three faults. Near the 207 mbsf fault, neither the IW nor the headspace gas data show significant excursions. In contrast, in the ~100 m thick section above the 610 mbsf fault, salinity, ammonia, and phosphate show substantial decreases, whereas sulfate shows an increase. Of the IW major elements measured, Ca and K are elevated above the fault and Na and Mg are decreased. The IW minor elements measured also show substantial changes within this interval, with Li, Si, Mn, and Sr increasing above the fault, wheras B, Ba, and Fe are depleted. Significant changes are also observed in the PBFZ, where the pH and chlorinity values abruptly decrease, whereas sulfate shows a dramatic increase to near-seawater values. Alkalinity, NH$_4$, PO$_4$, and Br show a continuous decreasing trend across the PBFZ depth with no discernible abrupt change, and the salinity data shows large scatters across the PBFZ. Notable changes in the major element concentrations include a decrease in Na and K, an increase in Ca, and scattered values of Mg in the PBFZ. Minor elements such as Li and Mn show a dramatic increase followed by an equally dramatic reduction within the PBFZ. The opposite is observed for B, which decreases first and then increases. Sr exhibits an increasing trend across the PBFZ. Fe and Ba are depleted around the PBFZ, likely due to more oxic conditions and presence of sulfate. Hydrocarbons (methane, ethane, and propane) measured from the headspace gas samples drop to near zero between 500 and 560 mbsf and again in the PBFZ. Hydrogen gas concentrations show significant spikes in both the 610 mbsf fault zone and the PBFZ, and there is a notable increase between 500 and 580 mbsf. Carbonate remains low as a result of being below the carbonate compensation depth (CCD).

Sampling and subsampling for microbiology were completed for Holes C0019J, C0019K, and C0019M. Whole-round samples were collected from 96 of the cores recovered, and residue from 19 IW squeeze cakes was also collected for comparison. In addition, 28 drill fluid samples and 100 core liner fluid samples were also collected to analyze samples for possible microbial contamination. Subsampling of whole-round cores was completed for Hole C0019J samples, and a minimized subsampling routine was applied to cores from Holes C0019K and C0019M. Although the majority of microbial analyses took place postexpedition, activity staining with Cell Tracker Green CFMDA was initiated onboard for 74 subsamples from Hole C0019J.

Observatory instrumentation was installed in two holes at Site C0019. An instrument string with 57 high-resolution temperature-sensing data loggers was installed into observatory Hole C0019D at 820.69 mbsf with sensors distributed between 692.96 and 819.75 mbsf. This observatory hole was previously drilled and instrumented during Expedition 343/343T in 2012. However, it no longer had instrumentation in it because the initially deployed string was removed in April 2013. The newly deployed instrument string was installed at the beginning of Expedition 405 to potentially observe hydrologic transients associated with drilling new holes, as well as to assess how the thermal field and previously observed hydrologic behavior have evolved. A second instrument string of temperature-sensing data loggers was installed in the newly drilled observatory Hole C0019Q to a depth of 902.89 mbsf. This string has 128 sensors distributed between 466.06 and 900.00 mbsf to characterize spatial and temporal variations in the subsurface hydrogeology. Retrieval of the instrument strings and their recorded data is anticipated to occur in later 2025.

7. Preliminary scientific assessment

The principal goal for Expedition 405 was to develop an integrated logging, coring, and borehole observatory approach to investigate the controls on large shallow slip on subduction zones, as was documented for the 2011 Tohoku-oki earthquake. The main objectives were as follows:

1. To constrain the stress field in the frontal prism region to evaluate the state of stress on the plate boundary fault and to evaluate the significance of stress changes since 2012;
2. To continuously core the input section at Site C0026 and frontal prism, décollement, and lower plate at Site C0019 to assess the structural development of the plate boundary fault system and how the structures might impact coseismic slip; and
3. To define the hydrogeologic structure in and around the PBFZ, frontal prism, and lower plate to develop new insight into the relationship between fluids and earthquake physics.

Overall, Expedition 405 was a huge operational success. Cores were recovered from multiple shallow HPCS holes at each site, as well as three deep SD-RCB holes at Site C0019 and one SD-RCD hole to ~300 mbsf total depth at Site C0026. Although the coring operations deviated slightly from the original plans due to the difficulties in penetrating thick sections of chert, the additional cores recovered proved to be extremely valuable. Together, the cores provide continuous records of the subsurface from the seafloor to the target depths corresponding to the deep sedimentary rocks and mafic volcanic rocks of the oceanic crust. Core recovery was generally very good, even for the deepest holes, and the core quality was excellent throughout. When combined with the high-resolution LWD data from one hole at each site, the results from Expedition 405 represent the first time that the entire section on the Pacific plate and at the frontal prism have been successfully sampled and characterized. Measurements and observations made during the expedition therefore provide a foundation for multiple new scientific results describing the processes associated with the PBFZ beneath the frontal prism. The range of applications of the data gathered during the expedition is vast, encompassing sedimentary and volcanic processes, paleoseismology, paleoclimate and paleoceanography, earthquake mechanics, and tectonic processes at convergent margins generally. Below, we summarize some of the preliminary scientific insights developed during Expedition 405.

7.1. First assessment of the temporal variation of stress in the frontal prism of a subduction zone

The ultrahigh-resolution borehole images acquired at Site C0019 are of excellent quality and allowed a detailed characterization of the borehole breakouts throughout the drilled section including at and beneath the plate boundary that can be compared with the equivalent Expedition 343 (JFAST) data. The prism data set is complimented by real-time images acquired from the input section at Site C0026, where few borehole breakouts can be inferred; they provide insights on stress in the outer-rise area.

At Site C0019, the main depth intervals of borehole breakouts observed during JTRACK are identical to those of JFAST, and occur between 300 and 420 mbsf and between 540 and ~760 mbsf. Moreover, the width, the azimuth, and the local variation of azimuth with depth, especially around the 610 mbsf fault, are very similar between the JFAST and JTRACK data sets. In addition, the physical properties inferred from logging measurements and from shipboard measurements on cores (porosity, seismic velocities, electrical, and thermal) from JFAST and JTRACK suggest no identifiable change in rock physical properties with time. Together, those observations imply that the stress state in the frontal prism has not changed in the 12 y between the two expeditions. The stress state at Site C0019 is still characterized by a very low deviatoric stress, mainly governed by the topography and the weight of the sediments, resulting in a normal fault regime with the maximal horizontal stress axis being 30° oblique to the convergence vector direction. At 823 mbsf, just beneath the top of the PBFZ, the maximum horizontal stress rotates by ~60°−70°, and the minimal horizontal stress becomes subparallel to the dip direction of the active normal faults bounding the horst and grabens in the downgoing plate.

At Site C0026, borehole breakouts of fair quality occur between 365 and 385 mbsf in the brownish dark clays. They indicate a mean maximum horizontal stress orientation of ~160°, 40° oblique from the convergence vector.

Anisotropy of magnetic susceptibility provides a time-integrated record of deformation across the fault, which is a product of the paleostress fields. The AMS fabrics at Site C0026 and below the plate boundary at Site C0019 are consistent with a sedimentary or compaction origin, with a K_{min} axis that is perpendicular to approximately horizontal bedding or foliation. The AMS fabrics above the plate boundary at Site C0019 are mostly consistent with horizontal shortening nearly parallel to the plate convergence direction. The contrast in AMS fabrics with depth at Site C0019 show that the plate boundary is decoupled from the geologic timescale, consistent with previous results obtained at the toe of the accretionary prisms (Housen et al., 1996; Ujiie et al., 2003; Yang et al., 2013).

This assessment of the present day stress field in the frontal prism and comparison with the Expedition 343 results directly addresses Objective 1 of Expedition 405. These preliminary results will be further expanded by postexpedition research to measure the relevant rock physical properties and potential time-dependent behaviors. Furthermore, numerical models with more developed rheological laws will be needed to evaluate the mechanical significance of the breakout data to develop more holistic interpretations of the current state of stress and how it may vary in space and time more broadly across the Japan Trench.

7.2. Structural characteristics of the plate boundary fault zone in the region of slip to the trench

Cores were recovered from the interval containing the PBFZ at Site C0019 from Holes C0019J and C0019K during Expedition 405. These two sets of cores, when combined with cores from Expedition 343 Hole C0019E and the LWD data from Expedition 343 Hole C0019B and Expedition 405 Hole C0019H, provide unique insight into the in situ structure of a PBFZ that generates great earthquakes.

The PBFZ separates the frontal prism above the décollement from the subducted Pacific plate below the décollement (Chester et al., 2013). The frontal prism consists of a series of hemipelagic

mudstones that are composed of substantial components of biogenic, volcaniclastic, and siliciclastic material. Biostratigraphic ages for the prism are all Pleistocene to Miocene. Deformation in the prism in the interval immediately above the PBFZ is minor, comprising minor faults, dark seams, and fractures. In all three cores (Holes C0019E, C0019J, and C0019K), the base of the prism, which corresponds to the upper contact of the PBFZ, is defined by a sharp transition in lithology from prism mudstone to an interval of clay-rich fault rock intercalated with mudstone. The top of the clay-rich layer is identifiable in the LWD logs from the corresponding excursion in the gamma ray measurements. The base of the PBFZ is coincident with the transition to color-banded clays in Holes C0019E and C0019J, where the color-banded clays show little to no evidence of deformation immediately below the deformed clay-rich fault rock interval. The color-banded clays are interbedded with and gradational to chert. These cherts exhibit significantly different physical properties from the overlying clays and muds and have the lowest gamma ray response of any of the lithologies and the highest seismic velocity of any of the sedimentary rocks. The character of the base of the PBFZ interval is similar for LWD Holes C0019B and C0019H, where the gamma response is consistent with an abrupt change from clay or mudstone to chert, which is interpreted to correlate to the top of the banded clay and chert in the cores. In Hole C0019K, the base of the PBFZ is less clearly defined. The base of the clay-rich fault rock is heavily disturbed by coring, such that the transition to the brownish black pelagic clay below is unclear. The brownish black pelagic clay stratigraphically overlies the banded clay and chert below in the input section at Site C0026, which is a sequence repeated at the base of Hole C0019K. However, the brownish black pelagic clay in Hole C0019K contains a penetrative scaly fabric, indicating strain within this sediment, and which may represent a gradational base to the PBFZ. Overall, the PBFZ is clearly defined in both cores and LWD logs. The PBFZ interval varies in thickness from ~1 to 15 m or more, depending on the interpretation of Hole C0019K, which indicates there is an order of magnitude of thickness variation that occurs over the tens of meters of lateral distance that separates the holes.

In cores from Holes C0019J and C0019K, the mudstone/clay contact at the top of the PBFZ was recovered intact. In both holes, there is a few millimeter–thick layer that is inferred to contain clay-rich gouge immediately below the contact. This gouge is evidence that shear deformation localized onto narrow principal slip zones. Within the fault zone, the presence of a fault contact is required at the contacts between an intercalated mudstone interval and sheared clay because there is a stratigraphic gap or reversal at these contacts. These contacts ubiquitously coincide with millimeter-thick layers of clay-rich gouge. The PBFZ in both Holes C0019J and C0019K also contains one or more additional localized slip zones. There are also several examples where there appears to be a sharp transition in clay composition (indicated by color) and/or fabric across a planar layer of what is likely clay-rich gouge, indicating slip zones localized within clay-rich material (similar to those documented in Kirkpatrick et al., 2015). Based on previous work that shows the clay in the PBFZ in Hole C0019E is smectite rich (Ujiie et al., 2013; Kameda et al., 2015), it is probable that the slip zones are also smectite rich. In this case, the PBFZ is likely frictionally weak (Ujiie et al., 2013; Ikari et al., 2015b), both statically and dynamically. Evidence of frictional heating during past earthquakes was identified from multiple slip zones in the PBFZ cores from Hole C0019E (Rabinowitz, 2020), suggesting the slip zones at the top of the PBFZ and within the PBFZ interval are likely to have accommodated seismic slip.

Further microstructural, geochemical, and paleomagnetic work is needed to confirm these interpretations. The cores recovered from the PBFZ during Expedition 405 provide an unprecedented opportunity to define the composition and structure of the PBFZ and to determine how the materials and structures within the PBFZ control fault mechanics, the main theme of Expedition 405 Objective 2.

7.3. Composition, structure, and tectonic evolution of the frontal prism

During Expedition 405, two sites were drilled that facilitate a direct comparison between the sedimentary inputs to the subduction zone and the architecture of the frontal prism and plate boundary fault system. This is the first time in the Japan Trench that both the entire frontal prism and underthrust section, as well as the undeformed input sediment sequence, have been cored/

recovered, providing new insight into the tectonic processes active in the shallow part of the subduction zone.

Cores recovered from Site C0026, located ~8 km seaward of the trench, contain hemipelagic muds, pelagic clay, and chert, which collectively represent a complete stratigraphic section of the sediments that overlie the oceanic crust of the Pacific plate. Biostratigraphic ages indicate the hemipelagic muds are recent to Early Miocene age and the underlying pelagic clay and chert are Early Miocene to Cretaceous age. The composition of the sediments and sedimentary structures preserved in these units are consistent with deposition in open marine, hemipelagic, and pelagic environments, with compositional variations and inferred sedimentation rates reflecting changes in terrigenous and biogenic input resulting from translation of Site C0026 toward the continental margin by motions of the Pacific plate over time (e.g., Moore et al., 2015). Physical properties measurements of porosity indicate a slight increase in compaction with depth, and deformation structures, although few, are mostly extensional faults. The geochemistry of the pore waters in the sediments suggest limited microbial activity at Site C0026, consistent with the observed extremely low TOC content, as well as potential fluid-sediment reaction or fluid-borne element transfer in the pelagic clay section. Overall, the input section appears to have undergone deposition, lithification, and compaction with little tectonic disruption.

Cores recovered at Site C0019 represent a continuous section through the frontal prism and PBFZ, as well as an upper portion of the lower plate. The units recovered from the prism above the PBFZ are Pleistocene to Late Miocene aged muds, which are compositionally similar to and broadly age-correlative with the Pleistocene to Late Miocene muds at Site C0026. Beneath the PBFZ, the sedimentary rocks are Early Miocene to Cretaceous pelagic clays and chert (with some mudstone intercalated with clay-rich fault rock in the PBFZ). Notably, lithologic equivalents to the Early Miocene and Cretaceous pelagic clays and chert were not recovered in the prism, and Pleistocene to Miocene ages muds were not recovered beneath the PBFZ. These observations appear to indicate that the uppermost ~150–200 m of the input section is offscraped into the prism and the lower ~50–100 m of sediments are subducted with the Pacific plate. However, there are several significant differences between the muds at the input site at Site C0026 and within the prism at Site C0019 that indicate additional sedimentary and deformation processes must contribute to prism formation processes. First, the sedimentary structures in the prism muds contain abundant evidence for soft-sediment deformation, including convolute bedding, block in matrix fabrics, slumps, and dewatering structures, which are absent in age equivalent muds at Site C0026. Second, multiple lithologic units in the prism contain shallow water ichnofacies and calcareous nannofossils, which are rare in the recent to Pliocene aged sediments at Site C0026. Third, TOC content and concentrations of hydrocarbon gases are both substantially higher at Site C0019 than at Site C0026. Collectively, these observations suggest the rocks that currently comprise the frontal prism are, at least in part, derived from sedimentary and/or tectonic reworking of the muds from the input section combined with a contribution of material sourced from landward of the prism.

Deformation structures recovered at Site C0019 reveal a structurally complex prism containing major fault inversions of sedimentary units, minor extensional and contractional faults, and potential folded sequences. Two major faults were identified in the frontal prism from biostratigraphic age reversals and structural observations. The shallower fault, present at ~207 mbsf, is defined principally from an age reversal, with Pliocene aged muds recognized overlying Pleistocene muds. The deeper fault at ~610 mbsf consists of a discrete gouge layer surrounded by breccias and damaged muds and in places Pliocene aged muds overlying Pleistocene muds. Pore water and headspace gas geochemistry show notable excursions in the interval above the 610 mbsf fault. Additional structural complexity within the prism is evident from bedding dips and paleomagnetic measurements. For example, bedding dip and inclination of the AMS fabric vary systematically from ~320 to ~510 mbsf, consistent with a broad fold coinciding with Lithologic Unit 4. Beneath the 610 mbsf fault, both bedding dips and AMS fabric are chaotic and show no systematic changes with depth. Minor faults and shear-offset structures with extensional or reverse senses of slip occur at all depths throughout the prism. Overall, these observations suggest the prism contains major faults that repeat the section by thrusting. However, the presence of minor faults with

apparent normal sense displacement suggest that the prism has also experienced extensional deformation.

The cores collected at Site C0019 during Expedition 405 clearly demonstrate that the frontal prism of the Japan Trench at this site is a complex and dynamic tectonic environment, which represents a significant contribution toward Objective 2 of the Expedition. Postexpedition research will further constrain the origins of the muds in the prism, the deformation kinematics and timing, the mechanical and hydrogeologic properties of the muds, and the controls on the patterns of pore fluid geochemistry, helping to develop a better understanding of how and why strain becomes localized in the plate boundary and frontal prism system.

7.4. Geochemical tracers of the hydrogeology of the frontal prism

Analyses of IW and headspace gas and rock samples from the two Expedition 405 sites provide high-resolution geochemical data that define and characterize the pore water fluids and how they vary with depth beneath the seafloor. These data enhance our understanding of the depositional, diagenetic, geochemical, and hydrogeologic processes occurring in the input sediments, and are highly valuable for understanding the dynamic hydrogeologic processes and architectural history of the shallow Japan Trench subduction zone.

At Site C0026, TOC concentrations within sediments from the incoming plate are very low, mostly less than 0.2 wt%. Sulfate values are elevated throughout the cored interval, demonstrating low levels of microbial activity except in the uppermost 15 m below the surface. Variations in the IW concentrations with depth and across lithologic units suggest some diagenetic addition and modification from an original seawater value. The most remarkable change is the trend to very elevated Ca concentrations, particularly in the brownish black clay in Unit 2. This exceptionally well-characterized geochemical data set not only enhances our understanding of hydrogeologic processes occurring in the incoming sediment but also provides a chemical fingerprint of the fluids found within the high porosity sediments of the incoming plate that will enter the subduction zone and prism. The low TOC can be coupled with onshore geochemical proxies to provide fundamental information for evaluating fluid and rock transport and redistribution by sedimentary and tectonic processes in the shallow portion of the PBFZ and the frontal prism.

IW and headspace gas analyses of Site C0019 samples provide high-resolution geochemical depth profiles over the entire 860 m thick section consisting of the frontal prism, PBFZ, and lower plate. The observed depth profiles reveal the presence of notable excursions in a tens of meters–wide interval above the 610 mbsf fault and within the PBFZ, which are both characterized by low IW salinity and alkalinity, and decreased concentrations of ammonium, phosphate, sodium, boron, iron, and methane, coupled with elevated concentrations of sulfate, calcium, and manganese. Relatively sharp gradients in the concentration profiles observed in the IW at these depth intervals are unlikely to be in a steady state but are controlled by dynamic processes. The excursion above the 610 mbsf fault appears to correspond to a zone of relatively high porosity, suggesting a close relationship between the excursion fluids and the evolutionary history of the frontal prism architecture. The IW geochemistry of the PBFZ is well constrained from samples recovered from Holes C0019J and C0019K and also JFAST Hole C0019E. The observed IW geochemistry profiles are essentially consistent with each other between these three holes at this depth interval, and are characterized by intense IW excursions. Significant similarities are observed between the excursion fluids at Site C0019 and those in the deeper units at Site C0026.

The geochemical results obtained during Expedition 405, supplemented and enhanced by postexpedition work, will be fundamental for characterizing the hydrogeology of the PBFZ and the frontal prism, which is the main theme of Expedition 405 Objective 3.

7.5. Composition of subducted basalt

The deepest hole drilled during Expedition 405 was Hole C0019P, from which SD-RCB cores were recovered from 930 to ~946 mbsf. The coring interval in Hole C0019P is over 100 m below the plate boundary fault at Site C0019 and was chosen to provide new insight on the deformation and geochemical processes that may be active deep beneath the subduction interface.

The rocks recovered in the Hole C0019P cores consist of a series of mafic rocks intercalated with sedimentary rocks of various compositions that confirm the predictions of a transition from sediments to a basalt/mafic igneous lithology at this depth from LWD data. The mafic rocks include a suite of pillow basalt, massive basalt, and dolerite, which exhibit a variety of textures indicative of extrusive and, potentially, intrusive origins. For example, curved edges with glassy rims observed in the shallowest basalt are interpreted to be rims of pillows. Amygdules are present in a zone that follows the curved outer edge of pillows. Brown limestone was sandwiched between the pillows, which contains fragmented glassy basalts in some places. The sedimentary rocks consist of gravels of red limestone, chert, and siliceous mudstone and basalt at the contact with sediment exhibits chilled margins. Mixing between lava and unlithified sediment is indicated by the apparent injection of veins of brown limestone mixed with hydrothermal minerals with the basalt. Beneath the sediments, altered basalt and massive dolerite were recovered that exhibit intrusive contacts with the sediments. Mesozoic radiolarians preserved in Units 2 and 3 in the deepest cores recovered from Site C0026 are consistent with the expected Cretaceous age of the oceanic crust at the Japan Trench from marine magnetic anomalies. These sediments overlie the basaltic crust, requiring the mafic rocks from Hole C0019P to be similar age or older.

The basaltic composition of the igneous rocks is characteristic of the oceanic crust, and the evidence for extrusive lavas is consistent with them representing the volcanic pile at the top of the oceanic crust. The presence of carbonate in amygdules and in the sedimentary rocks indicates formation of these units in relatively shallow water above the CCD. Together with textures indicative of mixing between lavas and sediments and the attitudes of some veins in the basalts being consistent with fracturing during cooling, the characteristics of these rocks all appear to be consistent with on-axis eruptive processes. Although the basalts are altered, preliminary observations indicate the alteration is predominantly associated with lava/sediment mixing zones and veins. There appears to be little evidence of alteration that may have occurred postsubduction. Furthermore, the pillows and sediments do not show evidence of substantial deformation, suggesting the basaltic crust, at least the portion recovered in these cores, has not been significantly involved in the deformation at the plate boundary.

8. Outreach achievements

Expedition 405 introduced a novel approach to outreach by including outreach officers from three international Program Member Offices (Australia-New Zealand IODP Consortium [ANZIC], European Consortium for Ocean Research Drilling [ECORD], and U.S. Science Support Program [USSSP]) and one Implementing Organization (IO)-managed effort (Japan Agency for Marine-Earth Science and Technology [JAMSTEC]) as part of its team on site. The goal of this program was to share the JTRACK science objectives to diverse domestic and international audiences, including scientists, students, educators, stakeholders, and the general public. During the expedition, outreach officers aboard *Chikyu* combined their diverse communication skills, including photography, videography, illustration, and journalism, to share science with broad audiences. Outreach activities included ship-to-shore broadcast events; interviews of science party members and crew; and publication of videos, blogs, magazine articles, and social media posts. Several projects began onboard and will continue into postexpedition activities. To date, there have been over 330 interviews, videos, comics, live events, blog posts, and other outreach efforts.

8.1. Ship-to-shore events

Using a direct satellite link (Starlink) and videoconferencing software (Zoom and Teams), outreach officers conducted 19 ship-to-shore events in five languages, reaching audiences in seven countries. Participants included a wide range of groups from elementary school students in afterschool robotics clubs to graduate students and public school teachers. Many of these events were conducted with international cultural institutions such as Miraikan National Museum of Emerging Science and Innovation in Japan and the American Museum of Natural History in the United States. Additionally, several science party members organized connections with their home institutions, providing unique insights into the expedition. In total, hundreds of people from around the world were able to connect virtually to *Chikyu* during Expedition 405.

8.2. Social media

JTRACK science, operations, and daily life were shared through frequent updates to official and personal social media accounts on X (formerly Twitter), Facebook, Instagram, LinkedIn, YouTube, and Bluesky. To date, hundreds of posts have been published to the JAMSTEC, ANZIC, ECORD, and USSSP social media accounts, reaching over hundreds of thousands of people and generating tens of thousands of engagements (reactions, comments, shares, and saves). A total of 24 videos have now been posted to the JAMSTEC YouTube channel and linked in a playlist, which altogether have been viewed over 8,000 times, with over 190,000 impressions.

8.3. Media coverage

Outreach through the mass media is one good way of providing an opportunity for a wide range of people to learn about scientific ocean drilling. Because the audience is wide-ranging, from those who are interested in science to those who are not, it is possible to reach out to new audiences. This will lead to an increase in interest and awareness of earth and planetary science.

Press offices for the institutions of all United States–based Window 2 science party members were contacted. To date, the story has been picked up by Cornell University, Stony Brook University, and University of California, Davis for dissemination in campus publications and wider media.

In Australia, preexpedition media released by The Australian National University on the participation of Australian scientists and outreach officers in the expedition included 116 media items across radio, print, and online, with a baseline audience of 317,173 by counting average readers per online article, total print circulation, and total broadcast audience. These items reached a total potential audience of 5,254,622.

Two issues (November and December) of the USSSP monthly digital newsletter, *the Drilling Dispatch*, were focused on Expedition 405. Coverage included articles with updates on science and operations, a feature about the installation of the borehole observatory, and spotlights on scientists and crew members involved in the expedition.

8.4. Additional outreach

8.4.1. Photography and videography

High-quality visuals can convey the wonder and complexity of scientific endeavors in ways that words alone cannot. Through these media, audiences can gain a tangible sense of the environments, working conditions, equipment, and people involved in groundbreaking research. For JTRACK, photography captured the essence of life aboard *Chikyu*, from the intricacies of scientific processes to the camaraderie of the team, offering a behind-the-scenes look at the expedition. Videography, on the other hand, brought motion and narrative to the forefront, documenting critical moments like core extractions, ship-to-shore broadcasts, and interviews with researchers. These media not only showcase the science but also humanize the scientists, making the work they do relatable and inspiring for diverse audiences.

The videography alone had high engagement rates across the numerous platforms across which it was published. These videos were further shared through additional partner and creator social media pages, including platforms such as LinkedIn, Instagram and Facebook, reaching additional audiences.

8.4.2. Sequential art

As part of the outreach initiatives for Expedition 405, a series of short comics were created specifically for a middle-grade audience. These comics covered topics such as traveling to and living on a research vessel, the collaborative dynamics of different research teams, the variety of geologic data studied, and the methods used for data acquisition. Designed to be visually engaging and easy to understand, the comics aimed to simplify complex scientific concepts and make the scientists behind the research approachable and relatable for kids.

8.4.3. Interviews

Interviews provide a direct connection to the individuals driving JTRACK's scientific success. Outreach officers conducted over 80 interviews with scientists, staff, operational personnel, and the crew of *Chikyu*. These interviews served diverse goals and reached audiences through various media.

Conversations with scientists–from early career to senior researchers–highlighted the human side of science in progress. These stories were aimed at inspiring broader audiences and potentially future generations to pursue a scientific career. Meanwhile, the success of JTRACK extended beyond researchers, relying on the dedication of a broad team. Interviews with crew members and behind-the-scenes experts shed light on the challenges, complexity, and collaborative effort underpinning this achievement. A third set, designed as oral history interviews, were aimed at documenting and preserving the collective legacy of scientific ocean drilling.

The interviews have been shared widely through various platforms: video interviews on social media, including YouTube and X; written interviews on institutional and personal blogs; and a mix of written and video formats in the Oral Histories of Scientific Ocean Drilling virtual repository.

8.4.4. Blog posts

Blog posts provide an opportunity for repeated interactions with researchers. Through these exchanges, writers can develop a deeper understanding of the research, allowing them to craft articles that are both accurate and enriched with meaningful context. This iterative process ultimately enhances the quality and impact of the written content. Science party members also manage their own personal blogs, where they describe a more personal experience of the science and culture of working at sea, as well as some of the details of their own scientific interests.

8.4.5. Journal articles

The article, "Deep-ocean drilling to explore the hydraulic structure of subduction faults" in *Nature Reviews Earth & Environment* offers an expert synthesis of the scientific findings and methods of Expedition 405 (Pei, 2024). It highlights the challenges of studying subduction faults at extreme depths and details the expedition's innovative techniques used to understand fault mechanics post-Tohoku-oki earthquake. This publication caters to an academic and professional audience, aiming to disseminate cutting-edge research outcomes to scientists, policymakers, and stakeholders involved in earthquake hazard mitigation.

The article "A Deep Dive into Subduction Zones and the Japan Trench" in *Frontiers for Young Minds* is designed to engage young audiences (8 to 12 year olds) by presenting the science behind Expedition 405 in an accessible and visually engaging format (Schuba et al., submitted). It simplifies complex concepts using relatable analogies and clear language. The goal is to spark curiosity and build foundational knowledge in the geosciences. By fostering early interest in geosciences, the article broadens the potential future talent pool for Earth Science research.

Additionally, articles have been pitched to popular science and adventure magazines including *New Scientist, Discover Magazine, Nautilus Magazine*, and *Sidetracked*, as well as the Geological Society of America (GSA) guest blog, *Speaking of Geoscience*.

8.4.6. Conference abstracts

The JTRACK science communication efforts for IODP are highlighted through presentations at major geoscience conferences, including the European Geoscience Union (EGU), American Geophysical Union (AGU), and Japan Geoscience Union (JpGU) annual meetings. These abstracts focus on innovative outreach strategies, such as the creation of comics and multimedia content tailored to middle-grade audiences, which aimed to make the complex goals and findings of JTRACK accessible and engaging. By sharing insights into the development and implementation of these communication tools, these presentations emphasized the importance of fostering public interest in geoscience research and inspiring the next generation of science, technology, engineering, and mathematics (STEM) professionals.

8.5. Postexpedition projects

8.5.1. Physical media: books

To showcase the stunning visuals captured during Expedition 405, plans are underway to produce a coffee table photo book and a glossy magazine. These high-quality publications will serve as striking, visual-only records of the JTRACK expedition, celebrating the beauty of the Japan Trench and the science conducted aboard *Chikyu*. The coffee table book will feature captivating seascapes, life aboard the research vessel, and detailed images of core samples and drilling operations, creating a lasting artistic tribute to the expedition. The glossy magazine will similarly highlight the expedition's essence through vibrant imagery, designed to engage diverse audiences and promote the groundbreaking work of JTRACK in a visually impactful way.

The comics created for Expedition 405 will be compiled into a compact, 48 page, A5 sized comic book specifically designed for middle-grade readers. This book will combine the illustrated short stories and at the end include photographs taken aboard *Chikyu*, offering a unique combination of engaging visuals and realistic depictions of life and work on a research vessel. The inclusion of still images alongside the comics will help ground the stories in reality, enhancing the educational value and authenticity of the content. Published in both English and Japanese, the comic book aims to reach a wide audience, inspiring children to explore the world of geosciences. By presenting complex scientific concepts in an accessible and relatable way, the book seeks to nurture curiosity, spark enthusiasm for Earth sciences, and encourage the development of a STEM identity at an early age. This initiative builds on Expedition 405's broader mission to make science approachable and to cultivate the next generation of scientists and innovators. Digital copies in English will also be made available on the *JOIDES Resolution* website, hosted by the USSSP.

8.5.2. Museum exhibitions

As of December 2024, the National Museum of Emerging Science and Innovation (Miraikan) is showcasing the results of the JFAST project. However, depending on the findings from JTRACK, it may be necessary to consider updating or replacing the existing exhibit.

The *Chikyu* exhibition could be further enhanced by incorporating the experiences and interviews gathered during the JTRACK outreach activities. Such additions would provide visitors with a richer and more comprehensive understanding of the vessel's role in advancing scientific exploration and the collaborative efforts behind these groundbreaking missions.

8.5.3. Curated video playlist for streaming

JAMSTEC has uploaded 24 short videos about the JTRACK expedition to their official YouTube channel as part of their science outreach efforts. The playlist covers a range of topics, including the technical aspects of deep-sea drilling, life aboard the research vessel, and interviews with scientists discussing their work and its broader implications. These videos provide accessible insights into the expedition's objectives and methodologies. To enhance the accessibility and viewer engagement, JAMSTEC has curated a dedicated playlist that consolidates all the videos related to JTRACK. This playlist simplifies navigation and it caters to diverse levels of interest and knowledge. It also ensures that the videos are readily available for English-speaking audiences, broadening the reach of the outreach efforts and enabling an international demographic to engage with the material.

8.5.4. Photo exhibitions

A curated selection of photographs was prepared for traveling exhibitions in collaboration with ECORD. These materials are intended to be made available for all ECORD program member offices and participating institutions. The photos can be printed individually depending on the exhibition location and purpose, for example in a research facility or for instance a "House of Science." In addition to the photographs, the traveling exhibition consists of accompanying material compiled by the ECORD Outreach Task Force for Expedition 405. The selection shows the drilling process as well as research on board, interchange between the scientific participants and the crew and life aboard *Chikyu*.

References

Argus, D.F., Gordon, R.G., and DeMets, C., 2011. Geologically current motion of 56 plates relative to the no-net-rotation reference frame. Geochemistry, Geophysics, Geosystems, 12(11). **https://doi.org/10.1029/2011GC003751**

Asano, Y., Saito, T., Ito, Y., Shiomi, K., Hirose, H., Matsumoto, Ta., Aoi, S., Hori, S., and Sekiguchi, S., 2011. Spatial distribution and focal mechanisms of aftershocks of the 2011 off the Pacific coast of Tohoku Earthquake. Earth, Planets and Space, 63(7):669–673. **https://doi.org/10.5047/eps.2011.06.016**

Brodsky, E.E., Mori, J.J., Anderson, L., Chester, F.M., Conin, M., Dunham, E.M., Eguchi, N., Fulton, P.M., Hino, R., Hirose, T., Ikari, M.J., Ishikawa, T., Jeppson, T., Kano, Y., Kirkpatrick, J., Kodaira, S., Lin, W., Nakamura, Y., Rabinowitz, H.S., Regalla, C., Remitti, F., Rowe, C., Saffer, D.M., Saito, S., Sample, J., Sanada, Y., Savage, H.M., Sun, T., Toczko, S., Ujiie, K., Wolfson-Schwehr, M., and Yang, T., 2020. The state of stress on the fault before, during, and after a major earthquake. Annual Review of Earth and Planetary Sciences, 48(1):49–74. **https://doi.org/10.1146/annurev-earth-053018-060507**

Brodsky, E.E., Saffer, D., Fulton, P., Chester, F., Conin, M., Huffman, K., Moore, J.C., and Wu, H.-Y., 2017. The postearthquake stress state on the Tohoku megathrust as constrained by reanalysis of the JFAST breakout data. Geophysical Research Letters, 44(16):8294–8302. **https://doi.org/10.1002/2017GL074027**

Byrne, T., Underwood, M.B., III, Fisher, D., McNeill, L., Saffer, D., Ujiie, K., and Yamaguchi, A., 2018. Geology and Tectonics of Subduction Zones: A Tribute to Gaku Kimura: Boulder, CO (Geological Society of America). **https://doi.org/10.1130/SPE534**

Chester, F.M., and Moore, J.C., 2018. Tectonostratigraphy and processes of frontal accretion with horst-graben subduction at the Japan Trench. In Byrne, T., Underwood, M.B., III, Fisher, D., McNeill, L., Saffer, D., Ujiie, K. and Yamaguchi, A. (Eds.), Geology and Tectonics of Subduction Zones: A Tribute to Gaku Kimura. Boulder, CO (Geological Society of America). **https://doi.org/10.1130/2018.2534(06)**

Chester, F.M., Rowe, C., Ujiie, K., Kirkpatrick, J., Regalla, C., Remitti, F., Moore, J.C., Toy, V., Wolfson-Schwehr, M., Bose, S., Kameda, J., Mori, J.J., Brodsky, E.E., Eguchi, N., and Toczko, S., 2013. Structure and composition of the plate-boundary slip zone for the 2011 Tohoku-Oki earthquake. Science, 342(6163):1208–1211. **https://doi.org/10.1126/science.1243719**

DeMets, C., Gordon, R.G., and Argus, D.F., 2010. Geologically current plate motions. Geophysical Journal International, 181(1):1–80. **https://doi.org/10.1111/j.1365-246X.2009.04491.x**

Expedition 343/343T Scientists, 2013. Site C0019. In Chester, F.M., Mori, J., Eguchi, N., Toczko, S., and the Expedition 343 Scientists, Proceedings of the Integrated Ocean Drilling Program. 343/343T: Tokyo (Integrated Ocean Drilling Program Management International, Inc.). **https://doi.org/10.2204/iodp.proc.343343T.103.2013**

Fujie, G., Kodaira, S., Nakamura, Y., Morgan, J.P., Dannowski, A., Thorwart, M., Grevemeyer, I., and Miura, S., 2020. Spatial variations of incoming sediments at the northeastern Japan arc and their implications for megathrust earthquakes. Geology, 48(6):614–619. **https://doi.org/10.1130/G46757.1**

Fujiwara, T., Kodaira, S., No, T., Kaiho, Y., Takahashi, N., and Kaneda, Y., 2011. The 2011 Tohoku-Oki earthquake: displacement reaching the trench axis. Science, 334(6060):1240. **https://doi.org/10.1126/science.1211554**

Fulton, P.M., and Brodsky, E.E., 2016. In situ observations of earthquake-driven fluid pulses within the Japan Trench plate boundary fault zone. Geology, 44(10):851–854. **https://doi.org/10.1130/G38034.1**

Fulton, P.M., Brodsky, E.E., Kano, Y., Mori, J.J., Chester, F.M., Ishikawa, T., Harris, R.N., Lin, W., Eguchi, N., and Toczko, S., 2013. Low coseismic friction on the Tōhoku-Oki fault determined from temperature measurements. Science, 342(6163):1214–1217. **https://doi.org/10.1126/science.1243641**

Hasegawa, A., Yoshida, K., and Okada, T., 2011. Nearly complete stress drop in the 2011 Mw 9.0 off the Pacific coast of Tohoku Earthquake. Earth, Planets and Space, 63(7):35. **https://doi.org/10.5047/eps.2011.06.007**

Hashimoto, C., Noda, A., Sagiya, T., and Matsu'ura, M., 2009. Interplate seismogenic zones along the Kuril–Japan trench inferred from GPS data inversion. Nature Geoscience, 2(2):141–144. **https://doi.org/10.1038/ngeo421**

Hirano, N., Machida, S., Sumino, H., Shimizu, K., Tamura, A., Morishita, T., Iwano, H., Sakata, S., Ishii, T., Arai, S., Yoneda, S., Danhara, T., and Hirata, T., 2019. Petit-spot volcanoes on the oldest portion of the Pacific plate. Deep Sea Research Part I: Oceanographic Research Papers, 154:103142. **https://doi.org/10.1016/j.dsr.2019.103142**

Hirano, N., Takahashi, E., Yamamoto, J., Abe, N., Ingle, S.P., Kaneoka, I., Hirata, T., Kimura, J.-I., Ishii, T., Ogawa, Y., Machida, S., and Suyehiro, K., 2006. Volcanism in response to plate flexure. Science, 313(5792):1426–1428. **https://doi.org/10.1126/science.1128235**

Housen, B.A., Tobin, H.J., Labaume, P., Leitch, E.C., Maltman, A.J., and Party, O.D.P.L.S.S., 1996. Strain decoupling across the decollement of the Barbados accretionary prism. Geology, 24(2):127–130. **https://doi.org/10.1130/0091-7613(1996)024<0127:SDATDO>2.3.CO;2**

Ide, S., Baltay, A., and Beroza, G.C., 2011. Shallow dynamic overshoot and energetic deep rupture in the 2011 M_w 9.0 Tohoku-Oki earthquake. Science, 332(6036):1426–1429. **https://doi.org/10.1126/science.1207020**

Iinuma, T., Hino, R., Kido, M., Inazu, D., Osada, Y., Ito, Y., Ohzono, M., Tsushima, H., Suzuki, S., Fujimoto, H., and Miura, S., 2012. Coseismic slip distribution of the 2011 off the Pacific coast of Tohoku earthquake (M9.0) refined by means of seafloor geodetic data. Journal of Geophysical Research: Solid Earth, 117(B7):B07409. **https://doi.org/10.1029/2012JB009186**

Ikari, M.J., Ito, Y., Ujiie, K., and Kopf, A.J., 2015a. Spectrum of slip behaviour in Tohoku fault zone samples at plate tectonic slip rates. Nature Geoscience, 8(11):870–874. **https://doi.org/10.1038/NGEO2547**

Ikari, M.J., Kameda, J., Saffer, D.M., and Kopf, A.J., 2015b. Strength characteristics of Japan Trench borehole samples in the high-slip region of the 2011 Tohoku-Oki earthquake. Earth and Planetary Science Letters, 412:35–41. **https://doi.org/10.1016/j.epsl.2014.12.014**

Ishii, M., 2011. High-frequency rupture properties of the Mw 9.0 off the Pacific coast of Tohoku Earthquake. Earth, Planets and Space, 63(7):18. **https://doi.org/10.5047/eps.2011.07.009**

Kameda, J., Shimizu, M., Ujiie, K., Hirose, T., Ikari, M., Mori, J.J., Oohashi, K., and Kimura, G., 2015. Pelagic smectite as an important factor in tsunamigenic slip along the Japan Trench. Geology, 43(2):155–158. **https://doi.org/10.1130/G35948.1**

Kanamori, H., Miyazawa, M., and Mori, J., 2006. Investigation of the earthquake sequence off Miyagi prefecture with historical seismograms. Earth, Planets and Space, 58(12):1533–1541. **https://doi.org/10.1186/BF03352657**

Kawagucci, S., Sakai, S., Tasumi, E., Hirai, M., Takaki, Y., Nunoura, T., Saitoh, M., Ueno, Y., Yoshida, N., Shibuya, T., Clifford Sample, J., Okumura, T., and Takai, K., 2023. Deep subseafloor biogeochemical processes and microbial populations potentially associated with the 2011 Tohoku-oki 3arthquake at the Japan Trench accretionary wedge (IODP Expedition 343). Microbes and Environments, 38(2). **https://doi.org/10.1264/jsme2.ME22108**

Kazama, M., and Noda, T., 2012. Damage statistics (Summary of the 2011 off the Pacific Coast of Tohoku Earthquake damage). Soils and Foundations, 52(5):780–792. **https://doi.org/10.1016/j.sandf.2012.11.003**

Keren, T.T., and Kirkpatrick, J.D., 2016. The damage is done: low fault friction recorded in the damage zone of the shallow Japan Trench décollement. Journal of Geophysical Research: Solid Earth, 121(5):3804–3824. **https://doi.org/10.1002/2015JB012311**

Kido, M., Osada, Y., Fujimoto, H., Hino, R., and Ito, Y., 2011. Trench-normal variation in observed seafloor displacements associated with the 2011 Tohoku-Oki earthquake. Geophysical Research Letters, 38(24). **https://doi.org/10.1029/2011GL050057**

Kirkpatrick, J.D., Rowe, C.D., Ujiie, K., Moore, J.C., Regalla, C., Remitti, F., Toy, V., Wolfson-Schwehr, M., Kameda, J., Bose, S., and Chester, F.M., 2015. Structure and lithology of the Japan Trench subduction plate boundary fault. Tectonics, 34(1):53–69. **https://doi.org/10.1002/2014TC003695**

Kodaira, S., Fujiwara, T., Fujie, G., Nakamura, Y., and Kanamatsu, T., 2020. Large coseismic slip to the trench during the 2011 Tohoku-Oki earthquake. Annual Review of Earth and Planetary Sciences, 48(1):321–343. **https://doi.org/10.1146/annurev-earth-071719-055216**

Kodaira, S., Nakamura, Y., Yamamoto, Y., Obana, K., Fujie, G., No, T., Kaiho, Y., Sato, T., and Miura, S., 2017. Depth-varying structural characters in the rupture zone of the 2011 Tohoku-oki earthquake. Geosphere, 13(5):1408–1424. **https://doi.org/10.1130/GES01489.1**

Kodaira, S., No, T., Nakamura, Y., Fujiwara, T., Kaiho, Y., Miura, S., Takahashi, N., Kaneda, Y., and Taira, A., 2012. Coseismic fault rupture at the trench axis during the 2011 Tohoku-Oki earthquake. Nature Geoscience, 5(9):646–650. **https://doi.org/10.1038/ngeo1547**

Koppers, A., and Coggon, R. (Eds.), 2020. Exploring Earth by Scientific Ocean Drilling: 2050 Science Framework: San Diego, CA (UC San Diego Library). **https://doi.org/10.6075/J0W66J9H**

Lay, T., 2018. A review of the rupture characteristics of the 2011 Tohoku-oki Mw 9.1 earthquake. Tectonophysics, 733:4–36. **https://doi.org/10.1016/j.tecto.2017.09.022**

Lin, W., Conin, M., Moore, J.C., Chester, F.M., Nakamura, Y., Mori, J.J., Anderson, L., Brodsky, E.E., and Eguchi, N., 2013. Stress state in the largest displacement area of the 2011 Tohoku-Oki earthquake. Science, 339(6120):687–690. **https://doi.org/10.1126/science.1229379**

Lin, W., Yamamoto, Y., and Hirose, T., 2023. Three-dimensional stress state above and below the plate boundary fault after the 2011 Mw 9.0 Tohoku earthquake. Earth and Planetary Science Letters, 601:117888. **https://doi.org/10.1016/j.epsl.2022.117888**

Moore, J.C., Plank, T.A., Chester, F.M., Polissar, P.J., and Savage, H.M., 2015. Sediment provenance and controls on slip propagation: lessons learned from the 2011 Tohoku and other great earthquakes of the subducting northwest Pacific plate. Geosphere, 11(3):533–541. **https://doi.org/10.1130/GES01099.1**

Nakamura, Y., Kodaira, S., Fujie, G., Yamashita, M., Obana, K., and Miura, S., 2023. Incoming plate structure at the Japan Trench subduction zone revealed in densely spaced reflection seismic profiles. Progress in Earth and Planetary Science, 10:45. **https://doi.org/10.1186/s40645-023-00579-7**

Nakamura, Y., Fujiwara, T., Kodaira, S., Miura, S., and Obana, K., 2020. Correlation of frontal prism structures and slope failures near the trench axis with shallow megathrust slip at the Japan Trench. Scientific Reports, 10(1):11607. **https://doi.org/10.1038/s41598-020-68449-6**

Nakamura, Y., Kodaira, S., Miura, S., Regalla, C., and Takahashi, N., 2013. High-resolution seismic imaging in the Japan Trench axis area off Miyagi, northeastern Japan. Geophysical Research Letters, 40(9):1713–1718. **https://doi.org/10.1002/grl.50364**

Purwamaska, I., and Fulton, P.M., submitted. Hydrologic thermal response tests: how borehole thermal response can constrain permeability. Geofluids.

Rabinowitz, H.S., Savage, H.M., Plank, T., Polissar, P.J., Kirkpatrick, J.D., and Rowe, C.D., 2015. Multiple major faults at the Japan Trench: chemostratigraphy of the plate boundary at IODP Exp. 343: JFAST. Earth and Planetary Science Letters, 423:57–66. **https://doi.org/10.1016/j.epsl.2015.04.010**

Rabinowitz, H.S., Savage, H.M., Polissar, P.J., Rowe, C.D., and Kirkpatrick, J.D., 2020. Earthquake slip surfaces identified by biomarker thermal maturity within the 2011 Tohoku-Oki earthquake fault zone. Nature Communications, 11(1):533. **https://doi.org/10.1038/s41467-020-14447-1**

Regalla, C., Bierman, P., and Rood, D.H., 2019. Meteoric [10]Be reveals a young, active accretionary prism and structurally complex décollement in the vicinity of the 2011 Tohoku earthquake rupture. Geochemistry, Geophysics, Geosystems, 20(11):4956–4971. **https://doi.org/10.1029/2019GC008483**

Remitti, F., Smith, S.A.F., Mittempergher, S., Gualtieri, A.F., and Di Toro, G., 2015. Frictional properties of fault zone gouges from the J-FAST drilling project (M$_w$ 9.0 2011 Tohoku-Oki earthquake). Geophysical Research Letters, 42(8):2691–2699. **https://doi.org/10.1002/2015GL063507**

Schottenfels, E., Regalla, C., and Nakamura, Y., 2023. Influence of outer-rise faults on shallow décollement heterogeneity and sediment flux at the Japan trench. Seismica, 3(1). **https://doi.org/10.26443/seismica.v3i1.386**

Schuba, C.N., Fulton, P., Kirkpatrick, J., Kodaira, S., Conin, M., Regalla, C., Ujiie, K., Pincus, M., Cooper, S., Bentley, C., and Expedition 405 Science Party, submitted. A deep dive into the Japan Trench. Frontiers for Young Minds.

Shipboard Scientific Party, 1980. Site 436: Japan Trench outer rise, Leg 56. In Scientific Party, Initial Reports of the Deep Sea Drilling Program. 56: Washington, DC (US Government Printing Office), 399–446. **https://doi.org/10.2973/dsdp.proc.5657.107.1980**

Strasser, M., Kölling, M., Ferreira, C.d.S., Fink, H.G., Fujiwara, T., Henkel, S., Ikehara, K., Kanamatsu, T., Kawamura, K., Kodaira, S., Römer, M., Wefer, G., R/V Sonne Cruise SO219A Scientists, and JAMSTEC Cruise MR12-E01 Scientists, 2013. A slump in the trench: tracking the impact of the 2011 Tohoku-Oki earthquake. Geology, 41(8):935–938. **https://doi.org/10.1130/G34477.1**

Tanikawa, W., Hirose, T., Mukoyoshi, H., Tadai, O., and Lin, W., 2013. Fluid transport properties in sediments and their role in large slip near the surface of the plate boundary fault in the Japan Trench. Earth and Planetary Science Letters, 382:150–160. **https://doi.org/10.1016/j.epsl.2013.08.052**

Tsuji, T., Ito, Y., Kido, M., Osada, Y., Fujimoto, H., Ashi, J., Kinoshita, M., and Matsuoka, T., 2011. Potential tsunamigenic faults of the 2011 off the Pacific coast of Tohoku Earthquake. Earth, Planets and Space, 63(7):58. **https://doi.org/10.5047/eps.2011.05.028**

Ujiie, K., Hisamitsu, T., and Taira, A., 2003. Deformation and fluid pressure variation during initiation and evolution of the plate boundary décollement zone in the Nankai accretionary prism. Journal of Geophysical Research: Solid Earth, 108(B8). **https://doi.org/10.1029/2002JB002314**

Ujiie, K., Inoue, T., and Ishiwata, J., 2016. High-velocity frictional strength across the Tohoku-Oki megathrust determined from surface drilling torque. Geophysical Research Letters, 43(6):2488–2493. **https://doi.org/10.1002/2016GL067671**

Ujiie, K., Tanaka, H., Saito, T., Tsutsumi, A., Mori, J.J., Kameda, J., Brodsky, E.E., Chester, F.M., Eguchi, N., and Toczko, S., 2013. Low coseismic shear stress on the Tohoku-Oki megathrust determined from laboratory experiments. Science, 342(6163):1211–1214. **https://doi.org/10.1126/science.1243485**

Valdez, R.D., II, Lauer, R.M., Ikari, M.J., Kitajima, H., and Saffer, D.M., 2015. Data report: permeability and consolidation behavior of sediments from the northern Japan Trench subduction zone, IODP Site C0019. In Chester, F.M., Mori, J., Eguchi, N., Toczko, S., and the Expedition 343/343T Scientists, Proceedings of the Integrated Ocean Drilling Program. 343/343T: Tokyo (Integrated Ocean Drilling Program Management International, Inc.). **https://doi.org/10.2204/iodp.proc.343343T.201.2015**

von Huene, R., Klaeschen, D., Cropp, B., and Miller, J., 1994. Tectonic structure across the accretionary and erosional parts of the Japan Trench margin. Journal of Geophysical Research: Solid Earth, 99(B11):22349–22361. **https://doi.org/10.1029/94JB01198**

Wang, D., and Mori, J., 2011. Rupture process of the 2011 off the Pacific coast of Tohoku Earthquake (Mw 9.0) as imaged with back-projection of teleseismic P-waves. Earth, Planets and Space, 63(7):17. **https://doi.org/10.5047/eps.2011.05.029**

Yang, T., Mishima, T., Ujiie, K., Chester, F.M., Mori, J.J., Eguchi, N., and Toczko, S., 2013. Strain decoupling across the décollement in the region of large slip during the 2011 Tohoku-Oki earthquake from anisotropy of magnetic susceptibility. Earth and Planetary Science Letters, 381:31. **https://doi.org/10.1016/j.epsl.2013.08.045**